UNLIMITED DISTRIBUTION

National Defence
Research and Development Branch

Défense nationale
Bureau de recherche et développement

A SURFACE PANEL METHOD FOR THE CALCULATION OF ADDED MASS MATRICES FOR FINITE ELEMENT MODELS

T.A. Vernon - B. Bara - D. Hally

February 1988

Approved by L.J. Leggat Director/Technology Division

DISTRIBUTION APPROVED BY

D/TD

TECHNICAL MEMORANDUM 88/203

Defence Research Establishment Atlantic

Centre de Recherches pour la Défense Atlantique

Canada

Abstract

A method of generating the added fluid mass matrix for use in dynamic analyses of submerged structures is presented. This method uses a distribution of panel singularities in the form of sources or dipoles on the fluid/structure interface to represent the velocity potential in the fluid surrounding the structure. The fluid added mass matrix is calculated by relating the pressure field in the fluid to the structure surface accelerations via the Euler equation and the assumptions of potential flow theory. Based on the results of a variety of investigations of computational performance, convergence and dynamic response involving floating cylinders, ship hulls, and propeller blades, the surface panel method is shown to provide an effective alternative to the finite element added mass matrix system. The surface panel program suite has been developed in a form compatible with an existing finite element analysis package, although the dependence on the particular solution system is not large.

Résumé

On présente une méthode de génération de la matrice des masses fluides ajoutées utilisée dans l'analyse dynamique des structures submergées. Dans cette méthode, une distribution de singularités de plaque sous la forme de sources ou de dipôles à l'interface du fluide et de la structure représente le potentiel des vitesses du fluide entourant la structure. La matrice des masses fluides ajoutées se calcule par association du champ de pression du fluide aux accélérations à la surface de la structure au moyen de l'équation d'Euler, dans le cadre des hypothèses de la théorie des écoulements potentiels. En se fondant sur les résultats de diverses études de performance de calcul, de convergence et de réponse dynamique menées à l'aide de cylindres flottants, de coques de navire et de pales d'hélice, on montre que la méthode des plaques de surface est un substitut efficace à la matrice des masses ajoutées à éléments finis. Une série de programmes de plaques de surface a été élaborée sous une forme compatible avec un actuel ensemble de programmes d'analyse à éléments finis, bien que la dépendance sur le système des solutions particulières ne soit pas grande.

Contents

Notation

$[A]$	Diagonal matrix of panel areas
$[C]$	Damping matrix
$\{F_f\}$	Fluid force vector
$\{F_s\}$	Structural and body force vector
$[H]$	Coefficient matrix relating source strength to velocity potential
$[K]$	Structural stiffness matrix
$[L]$	Coefficient matrix relating source strength to normal velocity at panel control points
$[M]$	Structural mass matrix
$[M_A]$	Added fluid mass matrix
$[T]$	Transformation matrix for normal to global directions
$[T_1]$	Transformation matrix for normal to x direction
$[T_2]$	Transformation matrix for normal to y direction
$[T_3]$	Transformation matrix for normal to z direction
$\{V_n\}$	Vector of control point normal velocities
$\{V_x\}$	Vector of control point x direction velocities
g	Acceleration due to gravity (9.81 m/sec^2)
G	Green's function
h	Mean depth of fluid
J	Reduction factor to account for 3-dimensional effects in strip theory solutions
L	Characteristic length of structure
n	Normal
p	Pressure

M_h	Added mass in heave
M_{sw}	Added mass in sway
M_{sg}	Added mass in surge
r	Separation of field and source point, radius of circle
r^*	Separation of imaged field and source point
t	Time
U	Free stream velocity (rigid body velocity) in x direction
U_∞	Characteristic free stream velocity in x direction
V	Free stream velocity (rigid body velocity) in y direction
W	Free stream velocity (rigid body velocity) in z direction
$\mathbf{x}$	field point coordinate vector (bold face)
$\mathbf{x}'$	structure surface point coordinate vector (bold face)
x'	local x coordinate in panel coordinate system
y'	local y coordinate in panel coordinate system
z	Height of free surface
Γ	Structure surface boundary
$\{\delta\}$	Nodal displacement vector
η	Surface wave amplitude
ρ	Density
σ	Source strength (assumed constant on a panel)
ϕ	Velocity potential function
ω	Characteristic circular frequency

1 Introduction

The prediction of the dynamic structural response of submerged structures requires a knowledge of the effect of the fluid on the structure. In the general case, the interaction leads to a complex coupled boundary value problem which is often of infinite extent. By applying certain assumptions justifiable for the lower vibration modes of most structures of interest, the interaction can often be uncoupled. In the simplest representation, the effect of the fluid on the structure will be proportional to only the interface accelerations, and thus can be included as an added mass component in the dynamic equilibrium equations of the structure. The added mass concept is exactly equivalent to an integral of the total kinetic energy which the body motion imparts to the surrounding fluid in a potential flow solution. For the numerical solution of the equilibrium equations by finite element methods, the added mass is in the form of a fully populated mass matrix which is combined with the structural mass matrix.

Several methods are available for the calculation of the added fluid mass matrix for finite element models. The most widely used is probably the finite element method itself, whereby the fluid surrounding the structure is discretized with finite elements similar to those used in solid element modelling, but usually based on a single variable per node, typically pressure or velocity potential. This approach has advantages in terms of compatibility, and as a variationally-based formulation, automatically provides a symmetric mass matrix. The symmetric form of both the mass and stiffness matrices is important, since it is exploited in the matrix algorithms of most finite element solver systems. The major disadvantages of finite element fluid modelling are the effort required in the generation of an effective fluid model and the larger CPU time and storage requirements necessitated by these large models. As well, for problems of infinite extent, the imposition of the far-field boundary condition at a finite distance in the finite element fluid model can adversely affect the solution. The use of infinite elements which incorporate singular shape functions provides a better representation of infinite domains, but the best accuracy is still obtained when these elements are combined with at least one layer of standard fluid elements, necessitating again a fluid model.

Since the interface surface is the only part of the structure in contact with a surrounding fluid, it is natural to try to formulate the interaction problem in terms of a boundary integral approach. This is possible using distributions of singularities on the body surface to represent the potential (or pressure) in the fluid surrounding the body. For closed structures, the boundary integral approach embodies assumptions about the fluid potential on either side of the interface surface. Different assumptions about the fluid potential inside the body lead to different formulations of the singularity-based methods, typically cast in discrete form as source or dipole distributions on panels on the interface surface. In the terminology of boundary integral methods, both types of singularity distributions can be

termed indirect or direct formulations, depending on whether the governing equations are written in terms of velocity potential or pressure respectively. In many other applications of boundary integral methods, the direct formulation tends to be more efficient; however, both approaches involve the same amount of computation in the calculation of added mass matrices. An example of the interpretation of the source formulation as a direct method can be found in Reference 1.

The method discussed here uses the well-known surface panel singularity distribution method originally presented by Hess and Smith[2], and since applied successfully in the solution of many problems in the potential flow regime. The necessary discretization of the body surface into quadrilateral panels lends itself well to use with finite element models where the fluid/structure interface elements can be interpreted as hydrodynamic panels. This approach has been discussed by Vorus and Hylarides,[3,4] and the theoretical development reported in this study follows their work closely. In addition, a simple reformulation of the integral equation in terms of a dipole distribution in place of the source distribution which forms the basis of their approach is shown to offer significant improvements in accuracy in certain cases, with no increase in computing time demand. As well, there do not appear to be any practical evaluations or comparisons of the results of the panel methods to experimental or finite element based mass matrix results in the literature. The objective of the current work has been to develop the surface panel method as a practical alternative to an existing finite element based fluid modelling capability, and to evaluate its performance more extensively by comparison with that method.

The surface panel method offers several important advantages over the finite element method in the generation of fluid mass matrices. First, fluid modelling is not required, which eliminates a large amount of data preparation and input; second, the formulation is much less CPU intensive and requires less file storage space; and third, the formulation is less susceptible to problems of element aspect ratio and size disparity. The disadvantages of the surface panel method are largely implementational in nature rather than theoretical, since effective structural modelling does not always provide adequate hydrodynamic modelling. In certain cases, problem specific coordinate and grid transformations are required. The surface panel method also produces an unsymmetric fluid mass matrix, which can affect the overall solution produced by a general purpose finite element solver system which exploits an assumed mass and stiffness matrix symmetry. The evaluation of the integrals in any boundary integral formulation also requires more effort than is typically necessary in a standard finite element approach.

Despite the apparent disadvantages, the potential savings in CPU time and the elimination of fluid modelling make the surface panel method extremely attractive. The report presents a theoretical outline for the surface panel method, and discusses its implementation as a direct substitute for the finite element fluid mass matrix routines within the existing finite element solution system VAST[5]. The method has been applied in the analysis of

several structures for which exact or comparison solutions are available. Rigid body added mass predictions are compared to an exact solution for a cylinder, and strip theory solutions for two frigate hulls. Natural frequency predictions using panel method fluid mass matrices are compared to results utilizing finite element based fluid mass matrices and to experimental results for a floating half-cylinder and for two propeller blades. The computer processing times for the fluid mass matrix generation for the two methods are also reported. Details of several of the major simplifying assumptions and the integral evaluation methods used in the surface panel formulation are presented as appendices.

2 Theory

A structural dynamic response analysis by finite element method requires the solution of the structural equilibrium equations in the form

$$[M]\ddot{\delta} + [C]\dot{\delta} + [K]\delta = F_f(t) + F_s(t) \tag{1}$$

In the presence of a surrounding fluid, the effect of the fluid on the structure enters through the forcing function $F_f(t)$, which in general embodies terms proportional to the structure's surface displacement, velocity, and acceleration. If fluid compressibility or a free surface is included, these terms become frequency dependent and without simplifying assumptions, the interaction is of a complex nature. For large structures, the vibration frequencies of interest are infra-sonic, and the effects of fluid compressibility are generally neglected. This frequency range, on the other hand, is often above the range in which free surface effects are significant. (A more detailed discussion of the assumptions associated with the free surface boundary condition is given in Appendix A). If damping and displacement proportional terms can also be neglected on the basis of order of magnitude, then the fluid forcing reduces to a pressure term proportional only to the surface accelerations of the structure. This extensive series of assumptions is commonly made in the dynamic analysis of large submerged structures, and is usually necessary to render such analyses tractable.

To obtain the fluid forces on the structure, the relationship between the fluid pressure field and the interface accelerations must be defined. This relationship can be determined via potential flow theory, in which a velocity potential function $\phi(\mathbf{x})$ satisfying the Laplace equation and appropriate boundary conditions is used to define the fluid flow field. For a structure vibrating in an infinite fluid domain, these boundary conditions are

$$\phi \to 0 \ \ as \ \ \mathbf{x} \to \infty \tag{2}$$

$$\left.\frac{\partial \phi}{\partial n}\right|_{\Gamma} = \frac{d\delta}{dt} \tag{3}$$

where Γ is the fluid/structure interface and the substantive derivative is used on the right-hand side of (3). If a free surface is present

$$\frac{d^2\phi}{dt^2} + g\frac{\partial\phi}{\partial z} = 0 \tag{4}$$

is the linearized free surface boundary condition to be satisfied.

A number of techniques can be employed to solve for the potential function which satisfies the above relations. In the surface panel method, function $\phi(\mathbf{x})$ is defined by a distribution of singularities of constant strength on panels on the interface surface. If a simple source distribution is used, the field potential at $\mathbf{x} = (x, y, z)$ is written in the form

$$\phi(\mathbf{x}) = \int_\Gamma G(\mathbf{x},\mathbf{x}')\sigma(\mathbf{x}')\, d\Gamma(\mathbf{x}') \tag{5}$$

where $\mathbf{x}'$ represents the coordinate vector of a point on the panel surface and σ is the source strength. In discrete form, (5) becomes

$$\phi(\mathbf{x}) = \sum_{j=1}^{NP} \sigma_j \int_{\Gamma_j} G(\mathbf{x},\mathbf{x}'_\mathbf{j})\, d\Gamma(\mathbf{x}'_\mathbf{j}) \tag{6}$$

where the constant panel source strength has been removed from the panel integral. The kernel function G in the current formulation is the free space Green's function for a source of strength of 4π

$$G(\mathbf{x},\mathbf{x}'_\mathbf{j}) = \frac{1}{r} = \frac{1}{|\mathbf{x} - \mathbf{x}'_\mathbf{j}|} \tag{7}$$

The gradient of the velocity potential function is then forced to satisfy the boundary condition of (3) at a number of control points on the body. In the current formulation, these control points are the panel centroids, Figure 1, and from equation (6), the gradient is given by

$$\frac{\partial\phi(\mathbf{x})}{\partial n} = \sum_{j=1}^{NP} \sigma(j) \int_{\Gamma_j} \frac{\partial G(\mathbf{x},\mathbf{x}'_\mathbf{j})}{\partial n}\, d\Gamma(\mathbf{x}'_\mathbf{j}) \tag{8}$$

The integrals in equations (6) and (8) can be evaluated exactly, and these analytical solutions are used when the panel-to-control point separation is relatively small. As the separation increases, an expansion can be used for the integral evaluation with little error. The calculation of these integrals is discussed in more detail in Appendix B. For a particular set of control points, the evaluation of the integrals in equations (6) and (8) leads to the system

$$\{\phi\} = [H]\,\{\sigma\} \tag{9}$$

$$\{V_n\} = [L]\{\sigma\} \tag{10}$$

with $[H]$ a coefficient matrix relating source strength to control point potential and $[L]$ a coefficient matrix relating source strength to control point fluid normal velocities. Relations (9) and (10) define completely the fluid flow field given the distribution of source strengths σ.

The fluid velocities normal to the panels at the control points can be related via equation (3) to the local nodal point velocities in the finite element model, using the four nodes which define a quadrilateral panel, Figure 1. For the complete system, this becomes

$$\{V_n\} = [T]\frac{d\{\delta\}}{dt} \tag{11}$$

In the current system, the transformation matrix $[T]$ contains factored direction cosines between the panel normal and the global axis system, with each node in the panel contributing 1/4 of the total. Equations (10) and (11) can be equated and rearranged to define the panel source strengths as

$$\{\sigma\} = [L]^{-1}[T]\frac{d\{\delta\}}{dt} \tag{12}$$

Substituting this expression into equation (9), we obtain an expression for the velocity potential at a control point in terms of the surface nodal point velocities

$$\{\phi\} = [H][L]^{-1}[T]\frac{d\{\delta\}}{dt} \tag{13}$$

An alternative formulation for the potential ϕ can be obtained by using a distribution of dipoles of constant strength on a panel. The solution for the dipole strengths then immediately provides the potential on the interface surface. In this case, the integral equation to be satisfied is

$$\int_\Gamma G(\mathbf{x},\mathbf{x}')\frac{\partial\phi(\mathbf{x}')}{\partial n}\,d\Gamma(\mathbf{x}') = \int_\Gamma \phi(\mathbf{x}')\frac{\partial G(\mathbf{x},\mathbf{x}')}{\partial n}\,d\Gamma(\mathbf{x}') \tag{14}$$

in which the derivatives of the velocity potential function are known. As in the source formulation, this can be cast in discrete form as

$$[H]\{V_n\} = [L]\{\phi\} \tag{15}$$

Solving for the control point potential and substituting for the surface velocities, we obtain

$$\{\phi\} = [L]^{-1}[H][T]\frac{d\{\delta\}}{dt} \tag{16}$$

Comparing this result with equation (13), it is evident that the only difference in the two formulations is a reversal of the order of the coefficient matrices in their product.

Because both approaches represent fundamentally exact solutions, both should converge to the same solution in the limit of infinite discretization. It is interesting to note that for certain structures, the added mass matrix obtained with a dipole formulation appears to be significantly more accurate than that obtained from the source formulation. Similar improvements have been discussed in the application of the panel methods to the study of potential flow about thin sections.[6]

The pressure field in the fluid of density ρ can be determined from the velocity potential via the Bernoulli equation

$$p = -\rho \frac{d\phi}{dt} \tag{17}$$

where again the substantive derivative is used. For example, substitution of equation (13) into (17) gives the panel control point pressures for the source formulation

$$\{p\} = -\rho[H][L]^{-1}[T]\frac{d^2\{\delta\}}{dt^2} \tag{18}$$

The pressure is integrated over the structure surface, in this case by a simple multiplication by the panel area to give the control point forces. These forces, which act in the normal direction to the panel, are separated into global axis components and distributed to the appropriate panel nodes via a transpose of the transformation matrix $[T]$. The complete expression for the nodal fluid force vector is then given by

$$\{F_f\} = -[T]^T[A][H][L]^{-1}[T]\frac{d^2\{\delta\}}{dt^2} \tag{19}$$

in which $[A]$ is a diagonal matrix of panel areas. Neglecting rigid body motion of the structure in the pressure and surface displacement derivatives, and nonlinear terms from the time derivatives, (see Appendix A) equation (19) reduces to

$$\{F\} = -[M_A]\ddot{\delta} \tag{20}$$

with $[M_A]$ a mass matrix in the form

$$[M_A] = [T]^T[A][H][L]^{-1}[T] \tag{21}$$

for the source formulation, and

$$[M_A] = -[T]^T[A][L]^{-1}[H][T] \tag{22}$$

for the dipole formulation. The terms in $[M_A]$ relate inertia forces at a surface node in a given global direction to unit accelerations in a global direction at a node. This mass matrix can be combined appropriately with the structural mass matrix in equation (1)

$$[M + M_A]\ddot{\delta} + [C]\dot{\delta} + [K]\delta = F_s(t) \tag{23}$$

If rigid body motion is retained in the structural displacements, additional terms proportional to the surface velocity and displacement are present in the nodal force vector (see Appendix A). The influence of these terms on the structural response does not appear to have been investigated, and is an aspect of this approach worthy of further study. Their influence is not considered further in this report since the added damping terms cannot currently be accounted for in the equilibrium equation solution system, and the added stiffness terms are of higher order in the displacements and are probably negligible.

The calculation of an added fluid mass matrix for a floating structure must involve the definition of the free surface. The technique of imaging is used in the surface panel method to define two forms of the free surface boundary condition as well as to define planes of structural symmetry. The symmetry option can be used to decrease the size of certain problems where that condition is applicable.

For the free surface, a pressure relief boundary condition is obtained by imaging a panel source distribution of opposite sign; a zero normal velocity surface condition is obtained by imaging a distribution of the same sign. Equation (7) becomes

$$G = \frac{1}{r} - \frac{1}{r^*} \tag{24}$$

or

$$G = \frac{1}{r} + \frac{1}{r^*} \tag{25}$$

for the two free surface conditions available. In practice, the pressure relief condition provides the correct approximation for most applications including all those discussed in this report. The structural symmetry condition is represented by the form (25).

3 Implementation

The calculation of the added fluid mass matrix for a finite element model forms a small part of the complete system required for dynamic analyses. The organization of a typical solution system is shown in Figure 2. Other than the necessary compatibility of surface geometry and details of the mass matrix format, both the finite element and surface panel method added mass systems are relatively independent of the particular analysis program. The objective of the current work was to develop a panel method as an exact equivalent to the existing finite element approach, which is discussed fully in Reference 7. Aside from a small increase in program operational commands in the surface panel method, the differences in the systems are largely transparent to the user. The differences in the input data requirements can be, of course, very significant.

3.1 Program organization

The panel method calculation of the added fluid mass is performed by the ADMASS program suite. The suite comprises four sections which must be run sequentially. Sections can be run independently, or combined as subroutines in a complete system. A brief description of each section is given here.

Section 1 (ADMS1) accesses the files containing structural geometry and finite element fluid and fluid/structure interface data, the format of which is described fully in Reference 5. These data are used to define the quadrilateral surface panels. The necessary panel properties are calculated (see Appendix B and Reference 8), checks are made on control point locations, and the properties stored. This section also defines the $[T]$ transformation matrix terms, although these are not stored specifically in the $[T]$ matrix form due to the highly sparse nature of that matrix.

Section 2 (ADMS2) reads the panel properties file and forms the influence coefficient matrices $[H]$ and $[L]$. The integral influence terms are evaluated either by an exact integration, a three term mulitpole expansion, or a single pole expansion, depending on the panel and control point separation. This routine is a modified version of the influence coefficient routine currently used in the program suite developed to predict the potential flow about ship hulls.[8] Further details are given in Appendix B.

Section 3 (ADMS3) computes the inverse of the potential coefficient matrix $[L]$. This system uses a block diagonal Gauss-Seidel iterative solution system which provides solution vectors within a prescribed error tolerance. This method has been found to be quite efficient as an in-core solver. The block size is currently a user-controllable feature, since this parameter can affect the inverse calculation efficiency and, to a lesser extent, the accuracy of the inverse matrix.

Section 4 (ADMS4) recovers the coefficient matrices, the panel properties and the transformation data and computes the added mass matrix given in equation (21) or (22). This matrix is stored as a binary disc file in the format required by the VAST program for addition to the structural mass matrix.

While the finite element method provides a symmetric added fluid mass matrix due to the variational basis of that formulation, the panel method does not. Since the VAST decomposition algorithm assumes symmetry in both stiffness and mass matrices, a post-processing symmetrizing option for the ADMASS system has been implemented (ADMSP). This system can again be run as a stand-alone program, or included in the complete mass matrix generation process. The current symmetrizing algorithm uses the simple formula

$$[M_A]_{sym} = \frac{1}{2}([M_A] + [M_A]^T) \tag{26}$$

which is equivalent to a least square minimization of the error in the off-diagonal terms. In practical applications, the differences in results between the symmetric and unsymmetric

matrices are not always significant since the mass matrices produced by the surface panel method are usually nearly symmetric.

All disc files accessed and created by the ADMASS system are binary format, with the exception of the nodal coordinate and interface element data files within the VAST system, and a panel property and diagnostic data file produced by the ADMS1 routine. These files are shown in the schematic of Figure 3. Specific details on the operation of the ADMASS system are given in Appendix C.

3.2 Operational constraints

Fundamental differences between the finite element and surface panel method of calculating added mass matrices impose certain operational constraints in the latter's application to finite element-based models. Several key requirements have been identified during the implementation and testing of the surface panel method, and these are discussed below.

3.2.1 Coordinate systems

The imaging planes used for free surface or athwartship symmetry plane definition in the ADMASS system are preset within the program; however, the added mass matrix is calculated in a coordinate system defined by the geometry of the structure. For analyses in which imaging planes are required, these internal and geometric coordinate systems must coincide in order that the mass matrix produced can be correctly combined with the structural mass matrix. In the current ADMASS system, the waterplane must be the origin of the global Z coordinate axis for free surface imaging, and the athwartship centerplane must be the origin of the global Y coordinate axis for symmetry imaging, Figure 4. There is no provision for longitudinal symmetry. Since this is not a conventional coordinate system for structural definition (but is effective for the imaging system), a geometry pre-processor shown as the first stage in the flowchart of Figure 3 has been developed for several of the typical structural coordinate systems. Note that the entire VAST analysis must then be done with the geometry in this new coordinate system. For analyses in which a free surface or symmetry plane is not required, no coordinate transformations are necessary.

3.2.2 Panel corner connectivity

A second operational constraint derives from the panel normal definition in the surface panel method. These are currently determined from vector cross-products of the panel diagonals, hence the panel nodal connectivity is critical to the correct orientation of the normal. To obtain correct normal orientation, a panel must be defined by a clockwise corner node order looking onto the structure from the fluid. If required, an option is available in the ADMS1 routine to reverse the complete set of panel node ordering from that read from

the element interface data file. The VAST interface elements which the ADMASS system is compatible with are shown in Figure 5. The correct nodal connectivity and the method of edge refinement for the 8-noded element are also shown in the figure.

Panel properties including areas, corner nodes and normal components can be verified in the ADMS1.DAT file produced by the ADMS1 routine, and it is suggested that this section be run as a stand-alone to obtain this file before the subsequent routines are run. The ADMS1 section is always the least demanding of the four sections in terms of CPU time, and rarely takes more than a few seconds to run.

3.2.3 Non-unique interface elements

A further operational problem arises when an interface element is connected to two fluid finite elements, one on either side, in the finite element model. This is equivalent to a zero thickness assumption, and is apparently adequate for added mass predictions by finite element method for relatively thin structures such as propeller blades. For the surface panel method, this modelling is not allowable, and each surface must be uniquely panelled. To this end, the ADMS1 routine offers several options to create the second surface, depending on the type of elements used in the structural modelling. In some cases, the added mass matrix computed from the two surface expansion must be condensed to eliminate the second surface. This operation has been included in the same post-processing system as the symmetrizing option. For further details of the program options, see Appendix C.

For cases in which a second surface cannot be defined with these options, the ADMASS system will not provide an added fluid mass matrix directly. A good approximation may be obtained by simply multiplying the fluid mass matrix determined with fluid on one side by a factor of two in cases where the surface normals on either side are approximately collinear.

4 Application and Evaluation

Subject to the constraints discussed in the previous section, the surface panel method provides an alternative capability for the calculation of added fluid mass matrices for a wide range of structural dynamics problems. It remains to evaluate the performance of the system in terms of the accuracy and efficiency of the method relative to the existing finite element system. There are a number of possible evaluation procedures; the simplest is to use finite element models of structures for which exact analytical results are available, such as cylinders and spheres, and to compare the exact results to the rigid body mass predictions (heave, sway and surge) from the panel method. These rigid body terms are obtained from a summation of appropriate terms in the fluid mass matrix. In this study, a half-cylinder has been used for this test. These results also provide a good indication of the convergence characteristics of the method as a function of the discretization of the structure

surface. As a second example of rigid body mass comparison, the heave and sway added fluid mass predictions for two ship hulls are compared to the predictions of strip theory using the Lewis form method. For the heave added mass, a comparison with a line dipole distribution method is also given.

Since the above comparisons involve only an integral of the added fluid mass, they reveal nothing about the distribution of the mass and its effect on the dynamic response solution. To better evaluate the characteristics of the complete mass matrix, a number of natural frequency analyses have been performed, utilizing first a fluid mass matrix generated via the finite element formulation, and secondly a number of fluid mass matrices from the surface panel method. In turn, these results are compared to experimentally determined natural frequencies. The examples considered for these comparisons are a floating half-cylinder and two different propeller blades.

4.1 Half-cylinder tests

The sectional added fluid mass in heave of a floating half-cylinder of radius r of infinite length is

$$M_h = \frac{1}{2}\rho\pi r^2 \tag{27}$$

and the sectional sway added mass is

$$M_{sw} = \frac{2}{\pi}\rho r^2 \tag{28}$$

The surge mass for the half-cylinder considered, with a length/radius ratio of 11.4, can be approximated adequately with the formula for ellipsoids[9]

$$M_{sg} = \frac{4}{3}k\rho\pi r^3 \tag{29}$$

with $k = 0.20$. For r =4.2 and L =96, the rigid body predictions from the ADMASS system should converge to the values

$$M_h = 2655 \quad M_{sw} = 1076 \quad M_{sg} = 61 \tag{30}$$

The added mass predictions from a series of tests with various circumferential disretizations of this cylinder are shown non-dimensionalized against the above values in Figure 6. A 10 panel longitudinal discretization of the model was used to obtain these results. Note that for these models with fluid on one side of the structure only, the same results are obtained from both the source and dipole formulations of the surface panel method.

It is evident that the convergence characteristics of the mass terms are different, with surge converging very quickly, and sway the most slowly. Sway appears to converge monotonically from above, while the heave predictions initially increase, then decrease through

the theoretical value. The errors arise from two main causes: the geometric approximation involved in a planar panel method which results in a poor representation of the true surface area of curved surfaces, and the fact that the control points are not on the true surface. Similar convergence characteristics were noted in Reference 3 for a two-dimensional source distribution method. It is stated there that the pressure terms are overestimated in the surface panel approach, causing the positive errors in the estimates of sway and heave mass. This may be the case in the ADMASS system as well, although the actual values of those terms have not been investigated. Based on these results, the convergence of the panel method appears to be quite acceptable. Tests with varying numbers of axial panels and the same circumferential discretizations as Figure 6 gave very similar values. This agreement correctly indicates the two-dimensional nature of the rigid body mass distribution for a long slender body.

The variety of discretization levels used in these and other tests have been used to construct the minimum CPU demand curve for the ADMASS system, presented in Figure 7. These times are for DREA's DEC 2060 machine and will vary a small amount depending on the operating load. The actual run-time will also depend on the convergence performance of the matrix inversion routine, which is monitored with an iteration counter in the ADMS3 routine. The curve in Figure 7 is based on a maximum iteration count of 2, which is almost always obtained for models with fluid on one side only. For thin submerged structures, the iteration count can be higher, and the CPU demand will increase accordingly.

The system has also been evaluated on a VAX 11-750 machine where CPU demand will average 2.2 - 2.5 times that shown in Figure 7. These CPU times do not include any post-processing time, as neither the symmetric nor condensed form of the added mass matrix is required for rigid body estimates. The current system utilizes several in-core solution algorithms for efficiency, thus imposing a limit on the matrix size which can be processed. For the DEC 2060, this limit is approximately 650 panels.

The rigid body estimates for any structure are obtained from the addition of all mass components in a particular degree of freedom in the added mass matrix. For the cylinder model for example, heave mass is obtained from the addition of every third element in every third row of the matrix. Sway and surge masses can be calculated similarly.

4.2 Ship hull added mass comparison

The ADMASS system has been used to compute rigid body added mass matrices for two frigate hulls for which comparisons can be made with the Lewis form method[10] and a line dipole distribution method.[11] The models used in these analyses were generated with a modified version of the hull surface generating routines developed for the prediction of potential flow around ship hulls.[12,13] This system produces half-hull models, which can be used with the centerplane symmetry option in the ADMASS system. To test this option,

Model	Discretization		DDH265 (tonnes)			CPF (tonnes)		
	Girth	Axial	Surge	Sway	Heave	Surge	Sway	Heave
Half-hull with	5	20	11.6	831	2314	19	1234	3820
x-z symmetry	8	20	11.6	785	2258	19	1163	3715
plane	10	25	11.6	776	2245	19	1157	3690
Full structure	10	20	23.4	1114	4634	37	1530	7600
Strip theory	Lewis form 21 stns		-	927	4280	-	1530	7140
	Dipole distribution		-	-	4208	-	-	7046

Table 1: Added fluid mass comparison for the DDH265 and CPF hulls.

the half-hull models were mirrored to obtain a full hull model, and results compared for the two approaches. The inverted full hull surfaces panelled with 200 elements are shown in Figures 8 and 9. The ADMASS results for both the DDH265 and Canadian Patrol Frigate are presented in Table 1, as are the estimates of added mass from the other methods. A consistent draft has been maintained in the various added mass evaluations. The Lewis form results were generated using the sectional area and half-beam and draft values for 21 stations on each of the hulls. Those predictions do not include a modal J reduction factor to account for three-dimensional effects.

These results indicate that the symmetry option correctly produces one-half of the total mass for the heave and surge directions. The sway results are incorrect for the half-models; however, the full model results are considered accurate. The cause of the discrepancy in the half-model results is under investigation. On the basis of this comparison, the surface panel method appears to overpredict the rigid body heave and sway mass with convergence from above, consistent with the results of the floating cylinder tests. The agreement in the results is quite encouraging, since these models represent relatively coarse grids. In the case of sway, the Lewis form methods are not considered to be particularily accurate; the panel method results for the full model are probably closer to the actual values.

4.3 Natural modes of a floating cylinder

To provide a more comprehensive evaluation of the characteristics of the added mass matrix produced by the panel method, the fluid mass matrices from the ADMASS and finite element formulation have been used in the natural frequency analysis of a floating half-cylinder. This finite element model also represents a physical model for which natural frequencies have been determined experimentally[14] for various drafts. The comparisons of the frequencies of this model for one draft are presented in Table 2. The finite element

Vibration Mode (N = node)	2 Layer F.E.M. Hz	Panel Method Hz	Experimental[14] Hz
2N Vertical	7.8	7.20	7.8
3N Vertical	20.8	19.8	21.3
4N Vertical	40.0	38.4	40.8
5N Vertical	64.1	62.6	65.8
2N Horizontal	7.8	7.20	7.8
3N Horizontal	30.8	13.5	16.0
4N Horizontal	36.6	25.4	27.8
5N Horizontal	52.7	41.1	43.8
1N Torsional	1.6	1.9	5.5
2N Torsional	36.6	37.3	41.5
3N Torsional	30.8	13.5	16.0
4N Torsional	52.7	25.4	27.8
5N Torsional	-	41.1	43.8
Mass (Kg)			
Surge	0.145	0.166	
Sway	4.37	5.55	
Heave	26.8	33.7	

Table 2: Comparison of natural mode predictions for a floating cylinder.

fluid model used two layers of 20-node fluid elements, and approximately 5.5 hours of CPU time were required to generate the added mass matrix. A three layer fluid model was also tested, which gave results very similar to those of the two layer model. This is consistent with finite element fluid modelling, in which two layers of quadratic elements will often adequately represent the infinite fluid domain. A three layer fluid model for this structure does not represent a particularly tractable problem due to the large CPU time required for the generation of the added mass matrix.

The rigid body added mass predictions for the two methods are also shown at the bottom of Table 2. The ADMASS system gives significantly higher rigid body added mass estimates than the finite element method; this is shown to be a consistent result in other comparisons of this nature. The ADMASS CPU time for the fluid mass matrix generation for this 168 panel model is about 4.5 minutes. The vertical natural frequency predictions utilizing either the finite element or surface panel method are in good agreement with the experimental results. The larger mass from the panel method indicated in the rigid body comparisons appears to result in a slightly low prediction of these vertical modes.

In the horizontal and torsional modes, the panel method mass results appear to provide better overall accuracy than those obtained with the finite element mass matrix. The exact cause of the poor performance of the finite element model in the prediction of these modes can probably be attributed to the complex coupling which occurs between the horizontal and torsional displacements, combined with the inability of the shell element used in the structural modelling to properly represent the shear stiffness distribution in this thin-walled structure. The differences between the results for the panel method mass matrix and the finite element mass matrix is a result of the sensitivity of this structure to the fluid mass distribution, which is a dominant component in the overall mass matrix.

It should be noted that, for this case and any other that utilizes the 8-noded interface element, the mass matrix produced by the ADMASS system is significantly smaller than that produced by the finite element method. This disparity results from the manner in which panels can be defined from elements which include mid-side nodes, Figure 5. The default option takes only the four corner nodes of this element, thus producing a mass component for only half of the interface nodes. An option to refine either edge of the basic grid using two of the mid-side nodes is available within the ADMS1 routine. This option then provides a mass component for 6 of the 8 nodes in each interface element. Currently there is no provision for a panelling which provides a mass component to all 8 nodes of the interface element, since this would require the creation of a new node within the panel. The contribution of that node would then have to be condensed out of the final added mass matrix before it could be combined with the structural mass matrix. Mass components for all interface nodes are provided when the 4-node interface element is used. For typical finite element grids, it is unlikely that a refinement further than that available will be required for accurate assessment of the added fluid mass. In the above example, the default option was used.

4.4 Natural modes of propellers

In a similar manner to the above example, the added mass matrices produced by the finite element and surface panel methods have been used in natural frequency analyses of two propeller blades. These models again provide a good comparison basis because of the large percentage of the total mass which stems from the fluid effects. Changes in this mass distribution thus have fairly evident effects on the natural frequency predictions. The first analysis is of a destroyer blade which has little skew and presents no particular modelling difficulties. The second is of an experimental, model-sized blade having very high skew. The finite element models of these blades are shown in Figures 10 and 11. A mid-surface view of the 3-dimensional fluid model is also shown surrounding the blades. The structural and fluid models were created with a propeller modelling program.[15]

4.4.1 Destroyer Blade

The destroyer blade served as a test case for the comparison of several different modelling options and discretization levels and for the evaluation of post-processing features within the ADMASS system. Two structural modelling options can be used in the current propeller modelling system: a shell element defined by 8 displacement nodes on one surface and 8 geometric nodes on the opposite surface, or a 20-node solid element.[5] Both of these models utilize the 8-node fluid/structure interface element, but only one surface of the blade is used as the interface, with fluid elements attached to either side of each interface element. This thin body assumption is not compatible with the surface panel method, but for either modelling option, it is possible to define the required second surface based on the geometry of the interface elements and a knowledge of the node numbering characteristics of the model generation routine.

In the case of the 20-node solid model, the resulting fluid mass matrix from the panel method is larger than that produced by the finite element method with the thin body assumption. That matrix can be combined directly with the structural mass matrix, since all nodes involved are displacement nodes. For the 16-node shell modelling option, mass components on the second surface are associated with geometric nodes, which are not included in the overall analysis. These mass components must therefore be condensed out of the total added fluid mass matrix by combination with the associated displacement node terms. A post-processing system to automatically perform this reduction has been developed and must be used before the added fluid mass matrix can be combined with the structural mass matrix. The reduction and symmetrizing options are available in the routine ADMSP described further in Appendix C.

The numerous comparisons for this propeller blade are summarized in Tables 3, 4, and 5. The results for the solid models are presented in Table 3, and those for the shell elements in Table 4. Results for the source and dipole formulations are also presented in those tables. The fluid model for the finite element added mass matrix for both models consisted of two layers of 20-node fluid elements, as indicated in Figure 10. A three layer model was also tested with one analysis of the shell model; those results were virtually identical to the predictions using the two-layer model, hence the latter is considered an adequate basis for comparison of accuracy and CPU time. Experimentally determined frequencies[16] are also shown in Tables 3 and 4.

It is evident that several of the measured frequency values are not predicted with the numerical models. The fourth and eighth modes are missed in all of the solid models, and the shell models miss the fourth mode in several cases. These defficiencies point out the sensitivity of the eigenvalue analysis to both the stiffness representation and the mass distribution for this structure. As can be seen in Table 4, the analysis of this blade using a more detailed grid of 80 shell elements (160 panels) gave a prediction for all of the

Mode	F.E. Mass	Source panel				Dipole panel		Exp[16]
	50	50	100 rad[1]	100 rad	100 chd	50	100 rad	
1	33	30	30	30	31	35	35	36
2	76	76	74	75	80	81	77	79
3	101	111	93	97	101	102	99	96
4	-	-	-	-	-	-	-	131
5	156	-	151	158	172	163	151	150
6	172	185	171	175	182	183	171	178
7	233	223	213	226	245	227	217	206
8	-	-	-	-	-	-	-	240
9	289	293	282	296	309	289	271	280
CPU sec[2]	1160	23	100	100	100	23	100	

[1] Unsymmetric form

[2] Mass matrix generation time only

Table 3: Comparison of natural mode predictions (in Hz) for the solid finite element model of the destroyer propeller blade; 'rad' and 'chd' refer to radial and chordwise respectively.

Mode	F.E. Mass	Source panel			Dipole panel			Exp[16]
	50	50	100 rad	160	50	100 rad	100 chd	
1	32	29	30	31	34	34	35	36
2	73	77	73	74	80	76	84	79
3	90	95	92	91	97	94	98	96
4	128	-	133	127	-	136	-	131
5	152	149	-	160	151	158	153	150
6	178	185	167	198	172	179	174	178
7	224	218	206	209	184	-	186	206
8	-	255	228	251	253	228	251	240
9	300	327	290	293	311	286	310	280
CPU sec[1]	1160	30	130	380	30	130	130	

[1] Mass matrix generation time only

Table 4: Comparison of natural mode predictions (in Hz) for the shell finite element model of the destroyer propeller blade.

experimentally determined modes. In general, the solution utilizing the finite element-based fluid mass matrix gave very accurate frequency estimates for these models. The best predictions were obtained when shell elements were used to model the propeller blade.

The results of six separate analyses to test the ADMASS fluid mass matrix with the solid model are presented in Table 3. First, several analyses using the source formulation were performed, starting with the unrefined finite element interface grid, which produces 50 panels, 25 on each face of the propeller. This mass matrix was used both in the unsymmetric and symmetric form for the source formulation. The results, which show inconsistent accuracy and missed modes, were the same for either form of the matrix. Two panel refinement options, a radial and chordwise refinement of order two, were also tested with the solid element model. It was anticipated that a radial refinement would be the more appropriate for a typical propeller blade because of the radially biased aspect ratio of the structure. The radially refined results do indicate slightly better agreement than those obtained with the chordwise refinement. The radially refined model was also tested in the unsymmetric and symmetric form. Again, no significant change in overall accuracy was obtained with the symmetric form, indicating that this is not a major disadvantage of the surface panel method. For consistency, all further runs utilized a symmetric form of the fluid mass matrix.

The frequency predictions for the fundamental mode using the source formulation form of the added mass matrix are somewhat low, indicating an overprediction of the added mass effect. This overestimate is evident in the rigid body added mass estimates produced by the source formulation, which are presented in Table 5. The mass estimates tend to decrease with increasing discretization, consistent with the convergence characteristics found in the half-cylinder tests, but are in general too high. The added mass estimates from the dipole formulation are in much better agreement with the finite element fluid mass estimates. Since the finite element method itself will overpredict the mass effect for a submerged body, these results indicate that the dipole formulation is the more accurate of the two panel method approaches for this structure. Two of the natural frequency analyses were repeated using the dipole form of the added mass matrix: the original grid and the radially refined grid. Those results, given in Table 3, provide improved accuracy for the lower vibration modes of this blade.

As one test to ensure that the refinement algorithm was functioning correctly, the rigid body fluid mass estimates from the radial refinement of the 50 panels to 100 panels was compared to a model which was generated with 50 elements (100 panels). These results are shown in Table 5, and indicate that similar, but not exact agreement is obtained. The small disparity is due to the slightly different panel grids which are produced by the two methods.

Table 4 presents the results of a similar series of analyses performed with the shell element models. The frequency predictions of the lower modes are again low due to the overprediction of the mass effect for this blade by the source formulation. The finite element-

Model	Source form mass (Kg)			Dipole form mass (Kg)		
	Surge	Sway	Heave	Surge	Sway	Heave
F.E. Mass	1020	337	20.7	1020	337	20.7
50 panels	1371	474	21.4	1044	391	23.0
100 chord	1247	437	22.1	952	360	21.8
100 radial	1319	446	23.3	1019	374	23.9
100 panels	1380	465	21.8	994	362	23.4
160 panels	1213	416	21.6	890	327	22.1

Table 5: Comparison of rigid body mass predictions from the finite element and panel method mass matrices for the destroyer propeller blade.

based fluid mass matrix and that from the dipole formulation of the panel method provide about the same overall accuracy, although modes are missed sporadically in both cases. Prediction of all experimentally measured modes was obtained with the more detailed shell model, at the expense of increased CPU time. These results have all utilized a symmetric form of the fluid mass matrix. The first four modal displacement contours for this propeller are shown in Figures 12 - 15 for the two fluid mass matrix options. The comparisons are based on the results from the shell finite element model for the case of the two-layer finite element fluid model and the 100 panel radially refined model using the dipole formulation (columns 2 and 7 in Table 4). The agreement between the results for the two mass matrices is very good for the lower modes. The frequencies of the higher modes are also predicted well with both forms of the fluid mass matrix, but the modal displacement contours begin to show differences. No experimentally determined modal displacement contours are available for comparison.

As discussed, the use of the symmetrized mass matrix has little effect on the modal predictions, and it is debatable whether this option is required, although it is not a demanding one in terms of CPU time. As the discretization level increases, the effect of the nonsymmetric form should decrease, although this has not been investigated in detail.

The CPU time requirements presented at the bottom of Tables 3 and 4 are indicative of the increased speed with which the surface panel method can produce the added fluid mass matrix, even when post-processing options are required. This post-processing can be a significant portion ($\sim$ 20 percent) of the total fluid mass matrix generation time. For the propeller analyses, the fluid mass matrix generation by finite element method takes approximately 50 percent of the total analysis CPU time. The reduction by a factor of 10 of that segment thus represents a large saving in overall time and cost. An even larger reduction ratio occurs for analyses on the VAX 11-750 machine, where processing times are

typically 2.5 times longer for any computationally intensive problems. These time estimates do not reflect any savings in model generation time, which is essentially negligible for the surface panel method, since it could work directly from the structural element definition for a submerged body such as the propeller. As well, the accuracy of the added mass matrix does not depend on the fluid modelling, which can present difficulties in automation for more complex geometries. The CPU time required for the overall analysis of the detailed model including the panel method added mass matrix was still significantly lower that that needed for analysis of the smaller models with the finite element fluid mass matrix.

4.4.2 DTNSRDC P4388 Blade

As a final comparison, a highly skewed, model-size propeller blade has been analyzed in a similar manner as described for the destroyer blade. This model represents a somewhat more complex geometry, and a grid of 45 shell elements (16 node option) has been used in the finite element model, Figure 11, in place of the 25 elements used for the destroyer blade. The results of these analyses are presented in Table 6. The unrefined and both chordwise and radial refinement results for the source formulation are compared to those utilizing a 2-layer fluid model for added fluid mass matrix creation, Figure 11, as well as to natural frequencies determined experimentally by holographic methods.[17,18] The results of analyses of the unrefined and radially refined models with the fluid mass matrix derived with the dipole formulation, and an analysis using 80 shell elements and a grid of 320 panels are also given in the table. In this case, the finite element method predicts a frequency which appears to have been missed in the experimental measurements.

The results for the lower modes of this blade are again quite encouraging for both the finite element-based and source formulation panel method fluid mass matrices. The predictions using the mass matrix based on the dipole formulation are poor, even for the lower modes. The higher mode predictions of all the analyses deviate from those determined experimentally; however, the agreement is within 10 percent for most modes, which is reasonable. The particularily poor performance of the dipole formulation here, in contrast to the better accuracy it provided in the previous example, is probably a result of the very small thickness of this propeller blade. Although this appears to contradict the suggestion that the dipole formulation offers increased accuracy for thin sections, it is probable that this model is approaching the limits for which any panel method could be expected to perform well. In these cases, the finite element-based added mass matrix may provide more consistent accuracy.

The rigid body added mass estimates for this blade for the various models are presented in Table 7. As could be anticipated from consideration of the frequency predictions, the dipole formulation significantly underestimates the dominant surge added mass component. The convergence characteristics for this blade are also inconsistent with previous results,

Mode	F.E. Mass	Source panel				Dipole panel		Exp[18]
	90	90	180 rad	160	320 rad	90	180 rad	
1	80	83	84	80	80	92	90	82
2	237	277	236	218	225	296	266	232
3	498	554	506	477	472	594	543	-
4	590	652	688	690	600	675	619	576
5	897	1026	919	857	849	1055	941	738
6	995	1121	1090	1079	956	1139	1017	930
7	1485	1703	1497	1360	1345	1765	1506	1245
8	1611	1851	1761	1633	1630	1843	1630	1600
CPU sec[1]	5900	115	535	380	2621	115	540	

[1] Mass matrix generation time only
All results based on a shell model

Table 6: Comparison of natural mode predictions (in Hz) for the DTNSRDC P4388 propeller blade.

Model	Source form mass (Kg)			Dipole form mass (Kg)		
	Surge	Sway	Heave	Surge	Sway	Heave
F.E. Mass	0.602	0.127	0.093	0.602	0.127	0.093
90 panels	0.569	0.133	0.117	0.465	0.114	0.097
160 panels	0.701	0.178	0.117	0.481	0.121	0.095
180 radial	0.667	0.158	0.118	0.502	0.175	0.126
180 chord	0.632	0.150	0.114	0.473	0.118	0.094
320 radial	0.666	0.155	0.123	0.472	0.120	0.090

Table 7: Comparison of rigid body mass predictions from the finite element and panel method mass matrices for the P4388 propeller blade.

again suggesting that the panel method is having difficulty with the geometry of this model. As well, the inaccuracy of the higher mode predictions in all the analyses indicates the sensitivity of the overall analysis to the numerical stiffness and mass representations. The results for the highly discretized model show improved accuracy, but the CPU time required for that analysis is unacceptably high.

Four of the modal displacement contours for this blade are presented in Figures 16 - 19. These comparisons are based on the finite element fluid model and the radially refined model (180 panels) with the source formulation fluid mass matrix. There is excellent agreement in the lowest two modes, but slight differences become evident in the higher modes. This again highlights the sensitivity of the analyses to the fluid mass distribution.

The CPU times for generation of the various fluid mass matrices used in the comparisons for this blade are shown at the bottom of Table 6. The times given for the surface panel method include the condensation and symmetrizing time. As was noted in the previous example, a saving of about an order of magnitude in CPU time can be obtained through the use of the surface panel source method in place of the two layer fluid models.

5 Concluding Remarks

The example applications have shown that the surface panel method is an effective alternative to the current method of finite element fluid modelling for the generation of the added fluid mass matrix. In all cases, the surface panel method provided a fluid mass matrix which gave similar accuracy for the lower vibration modes in significantly less CPU time than that required for matrix generation via the finite element method. For moderately thin submerged structures such as full scale propeller blades, the dipole formulation of the surface panel method provides better overall accuracy than the source formulation. For very thin structures, the reverse appears to be true, and the finite element method, in conjunction with a thin body assumption, will probably provide more consistent accuracy than either form of the surface panel method.

The rigid body added mass estimates from the surface panel method for the structures with fluid on only one side indicate that the method will overpredict the added mass effect, and converge with increasing discretization from above the exact value. This results in a convergence from below for the lowest vibration modes. The overprediction has little effect on the higher vibration modes. For moderately thin, submerged structures, the convergence characteristics follow similar trends, but tend to be more sensitive to the panel geometry, and may show inconsistencies. It is suggested that this dependence on interface geometry is no more severe than that for the finite element method for such structures, although that sensitivity has not been investigated in detail in the current work. For very thin structures, these inconsistencies can be acute, particularily for the dipole formulation. The use of finite

element-based added mass matrices will provide greater accuracy in these cases, since that method, in conjunction with the thin body assumption, will not be affected by changes in the structural thickness.

A finite element grid adequate for vibration analyses of the structure in air generally provides a definition of hydrodynamic panelling adequate for the prediction of the lower vibration modes of the structure in water. For accuracy in the higher mode predictions, refinement of the basic grid will be required. This refinement may have an adverse effect on the convergence performance of the coefficient matrix inversion algorithm for structures with reasonably complex geometry. The convergence performance can usually be improved by increasing the user-controlled block size in that routine.

The lack of symmetry in the fluid added mass matrices generated with the surface panel method appears to have little effect on the accuracy of the vibration mode predictions for the structures analysed. A simple and non-CPU-intensive symmetrizing algorithm can be used which provides a slight increase in overall accuracy.

For the models considered, the CPU time ratios for the finite element method versus the panel method varied from a minimum of approximately 10 in the propeller analyses, to a maximum of about 70 for the floating cylinder. This ratio is necessarily very dependent on the fluid model used for the comparison, but in general, a CPU time reduction of at least an order of magnitude can be expected using the surface panel method. For large and/or complex structures for which the necessity of fluid modelling has previously hampered the analyses, the surface panel method may provide an effective fluid mass modelling capability.

Several aspects of the surface panel method for added fluid mass prediction could be examined in more detail or developed to provide increased accuracy. Typically, higher accuracy will come at the expense of increased computation time. Two general areas are suggested for further investigation and development:

1. the development of more flexible methods of defining panels from finite element grid data, and;

2. the incorporation of a more general Green's function in the evaluation of the influence coefficients.

Addressing the first point, a large part of the development of a practical panel method system has involved the conversion of finite element grid specifications to effective hydrodynamic panelling. Further effort could be directed at providing more flexibility in the panel definition in terms of both refinement and enlargement options, since there is no requirement that the elements and panels be related on a one-to-one basis. Refinement beyond the level currently available in the system will create additional nodes, for which the mass contribution will have to be condensed out of the final fluid mass matrix. This option would allow the generation of a fluid mass matrix with mass contributions for all

nodes of the 8-node interface element. An enlargement option might be convenient in cases where a detailed model created for stress analysis is used in a vibration analysis, where such refinement may not be required.

The second important area of further research involves the replacement of the simple free space Green's function with a frequency dependent function which accounts for the presence of waves on the free surface.[19,20] The implementation of that option from a programming viewpoint would be quite straightforward, although the more complex function will require a numerical integration algorithm in addition to the exact and multipole methods exploited in the current system. It is anticipated that this approach would have adverse effects on the computational efficiency of the panel method system, but could increase the accuracy in cases where free surface effects are important.

In conclusion, the inherent advantages of the surface panel method for added mass matrix calculation can be realized within a finite element-based analysis system. With the exception of very thin structures, the panel method should provide an effective alternative to finite element modelling of infinite fluid domains.

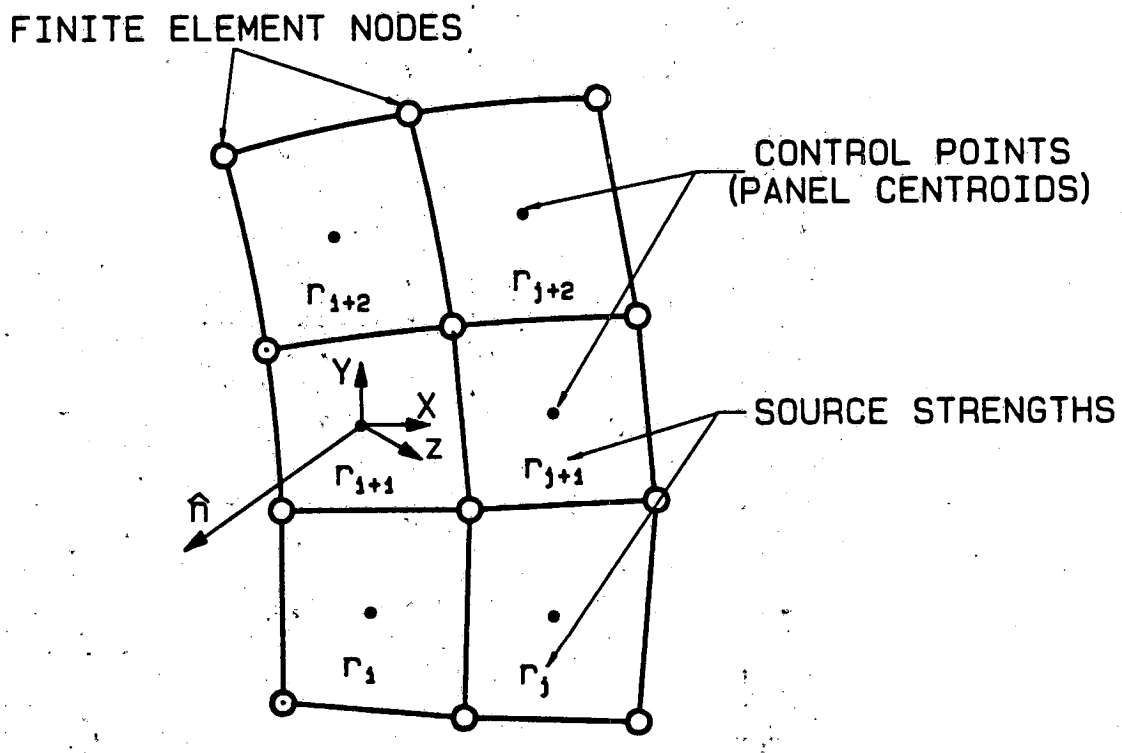

Figure 1: Surface panel nomenclature and representation.

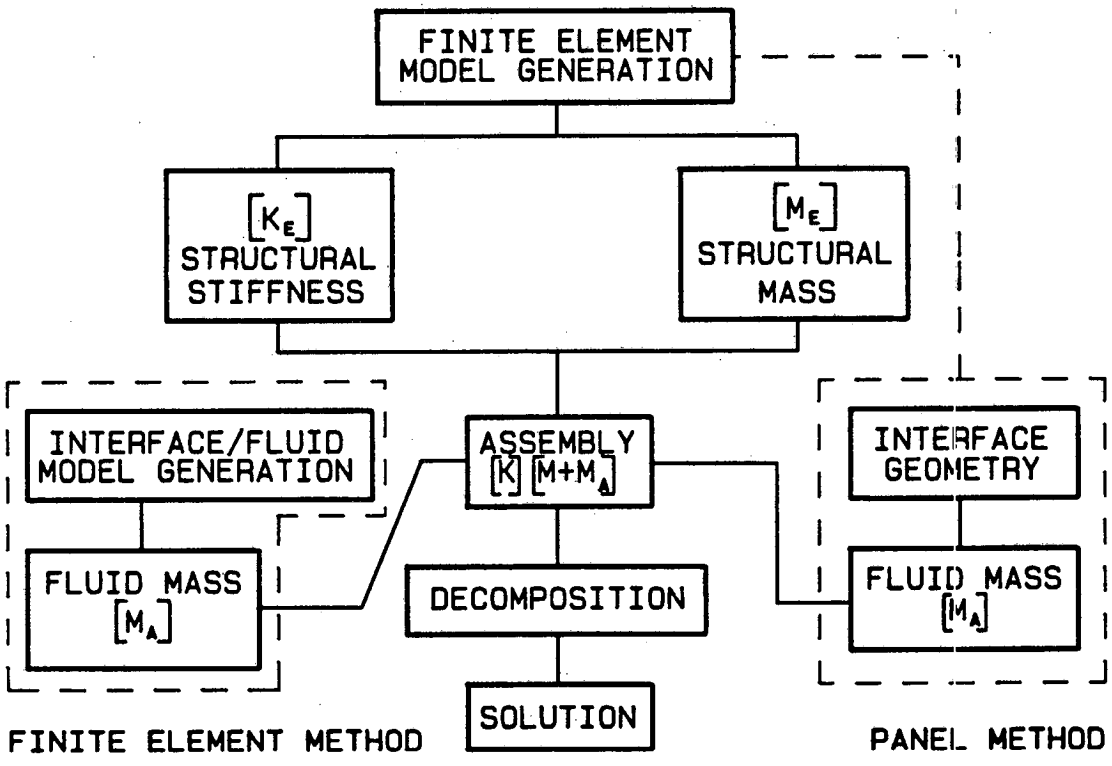

Figure 2: Dynamic response analysis flow chart for structures requiring added fluid mass evaluation.

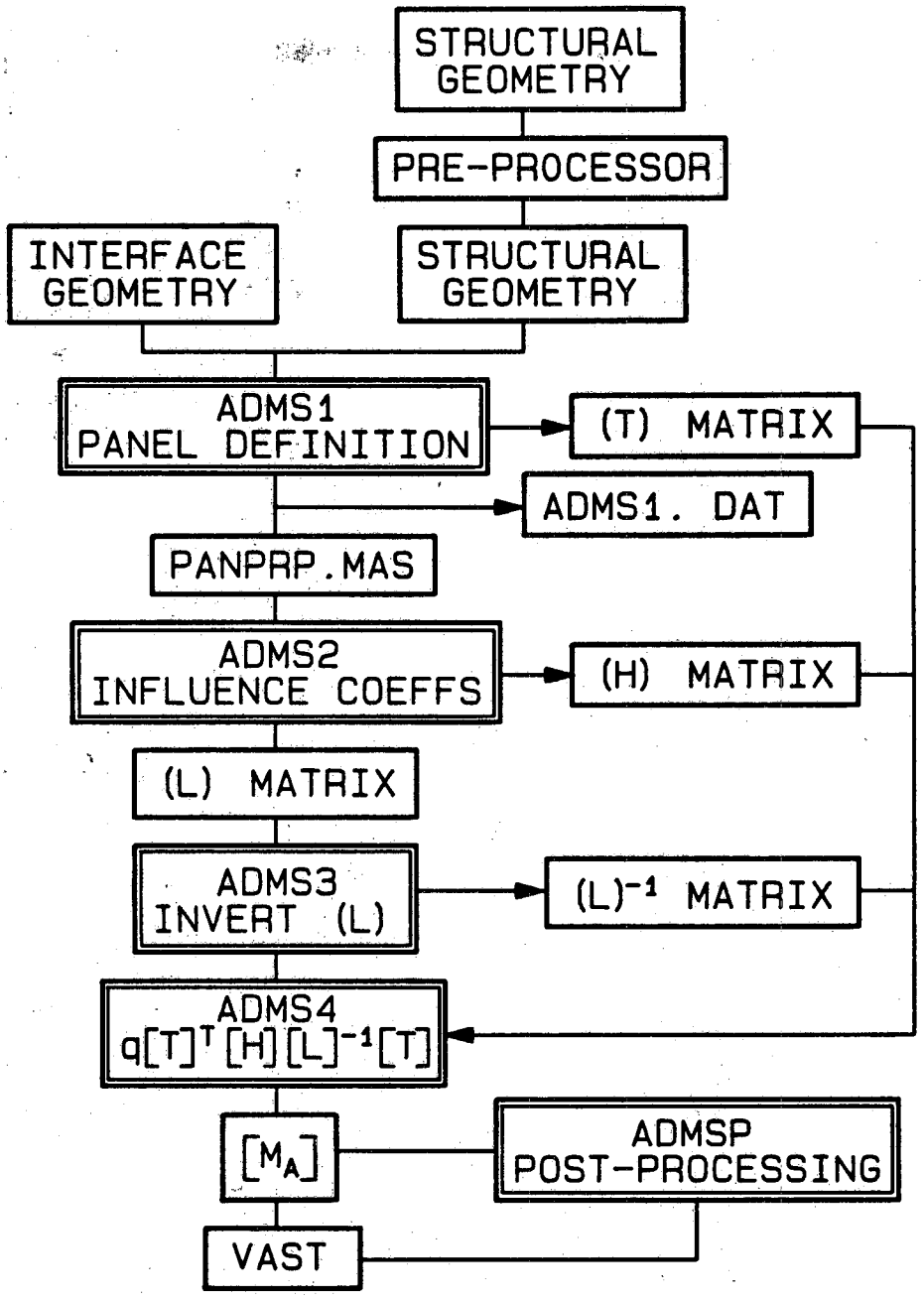

Figure 3: ADMASS system flowchart.

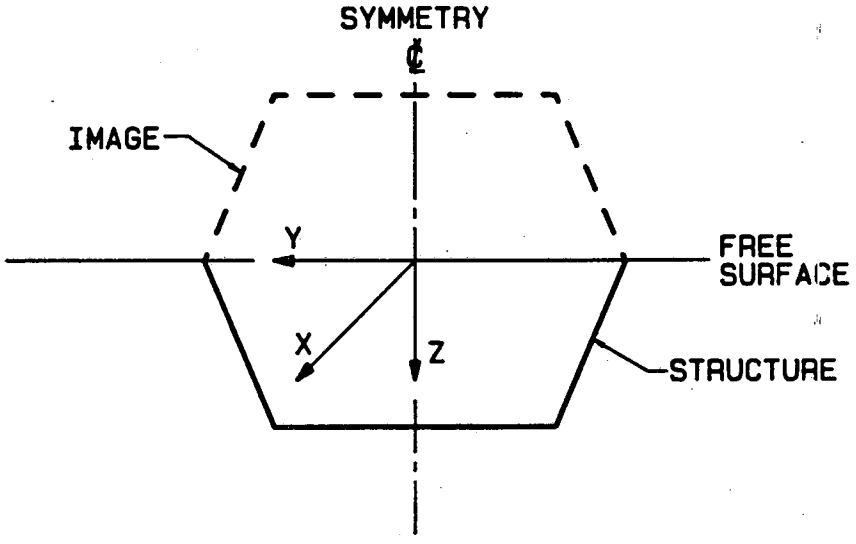

Figure 4: Internal coordinate system for imaging in the ADMASS system.

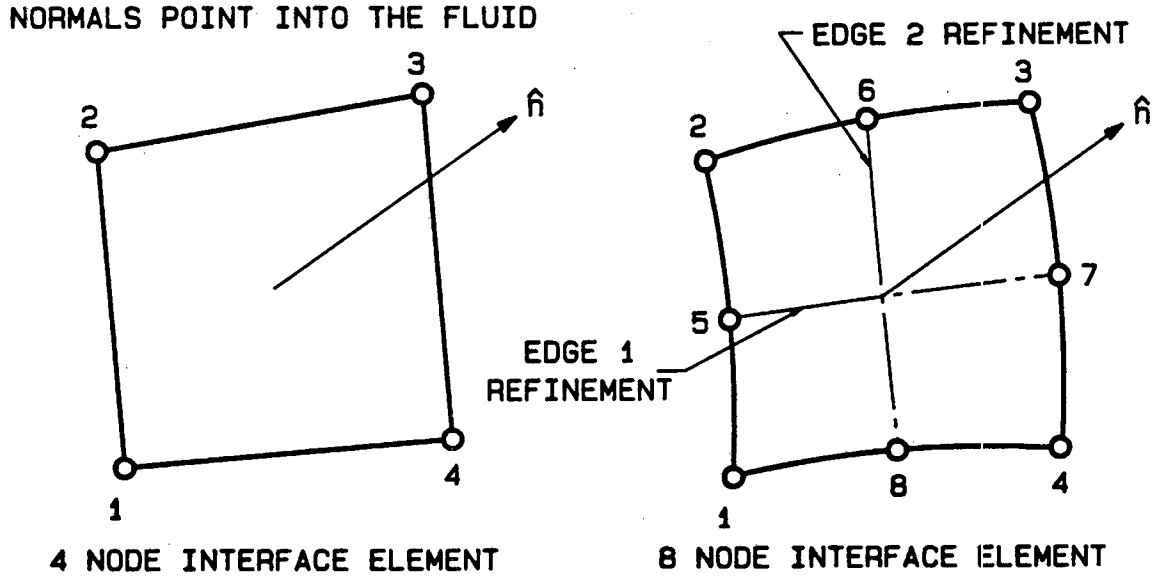

Figure 5: Interface elements, nodal connectivity and refinement options for the ADMASS system.

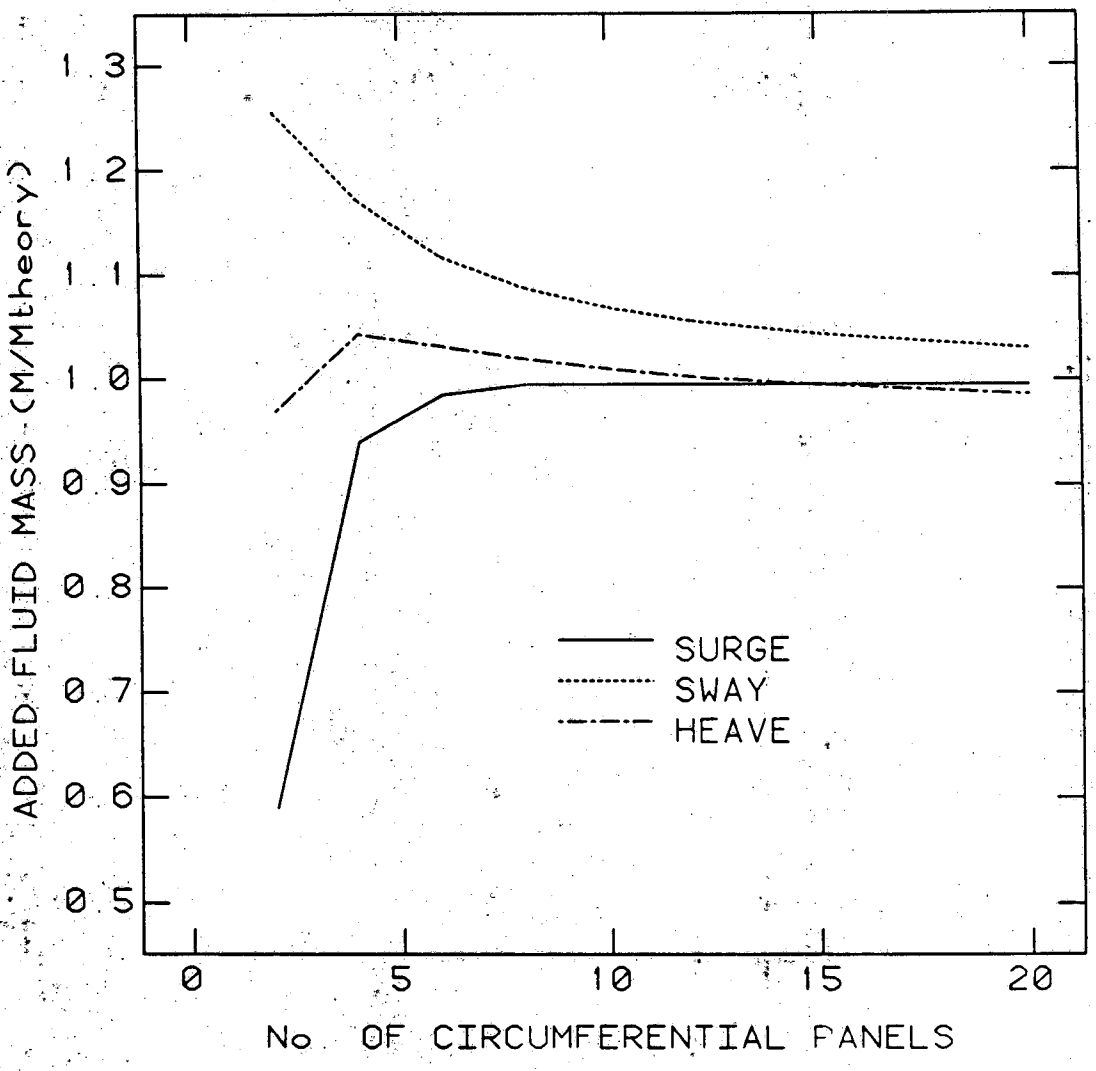

Figure 6: Rigid body mass convergence for a half-cylinder as a function of circumferential discretization.

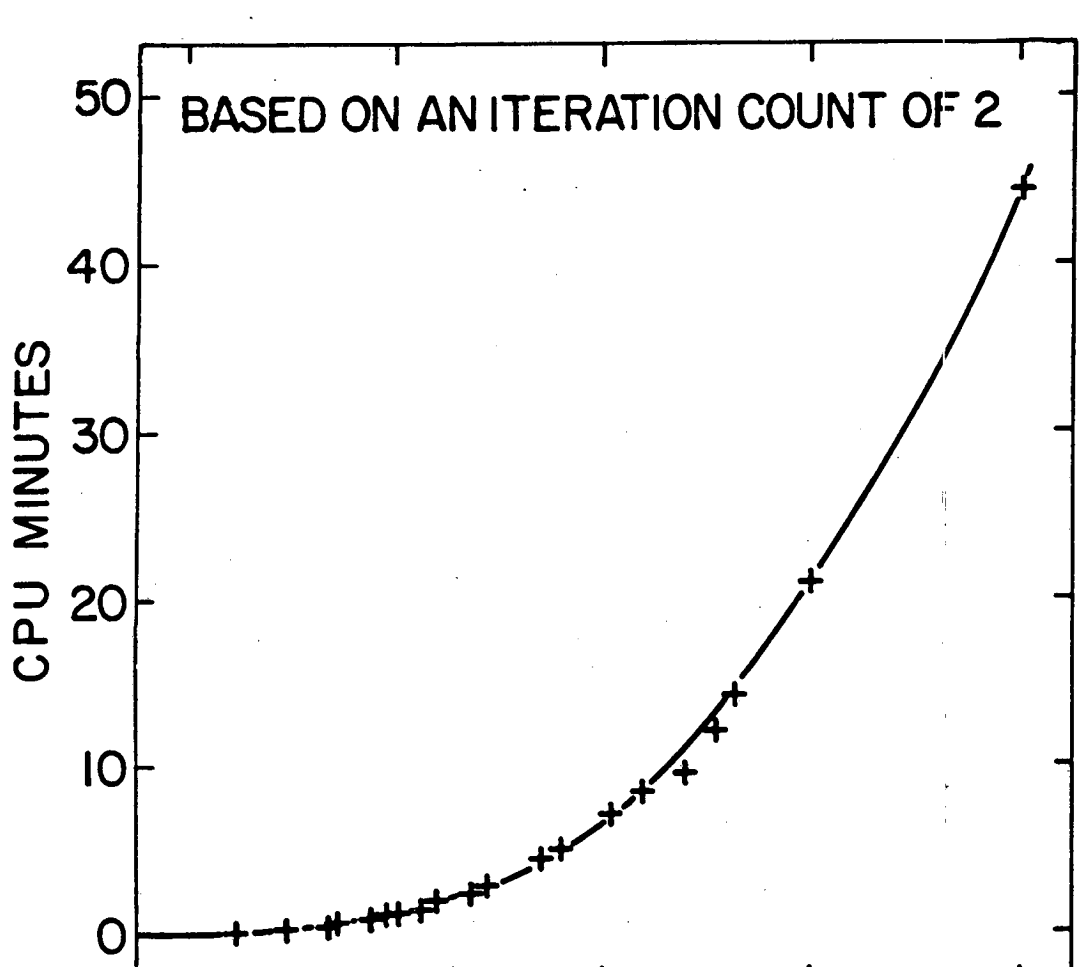

Figure 7: Minimum CPU time demand for mass matrix generation as a function of the number of panels (DEC 2060). For VAX 11-750, CPU times increase by approximately 2.5 times.

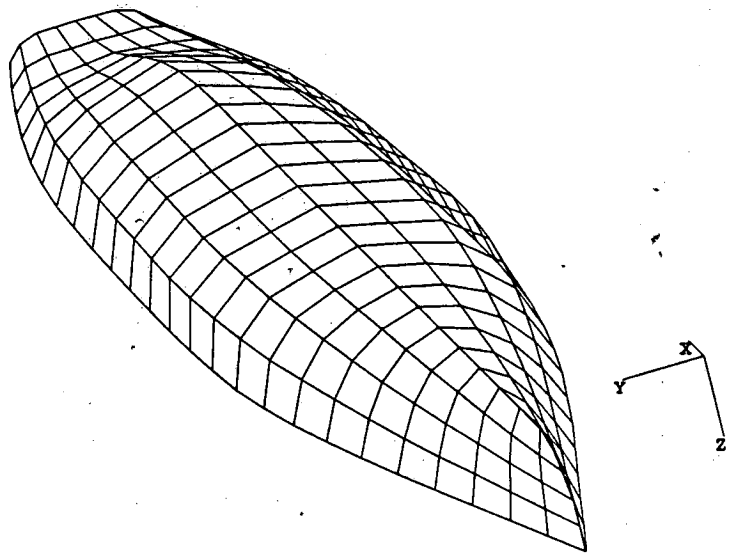

Figure 8: Panel representation of the DDH265 destroyer hull for added mass evaluation.

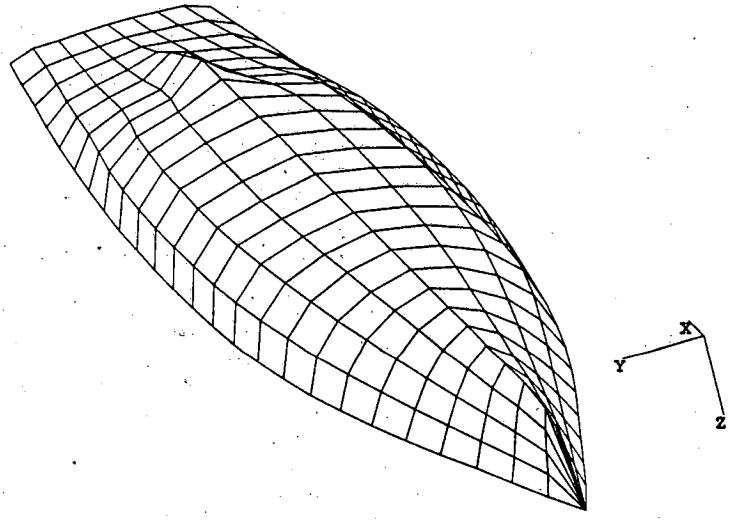

Figure 9: Panel representation of the Canadian Patrol Frigate hull for added mass evaluation.

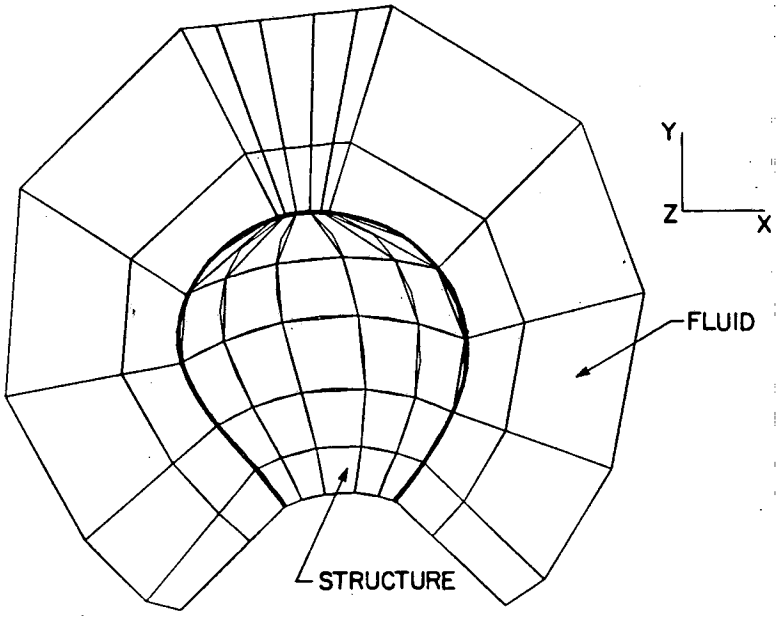

Figure 10: Finite element model of a DDH destroyer propeller blade with a two layer fluid model.

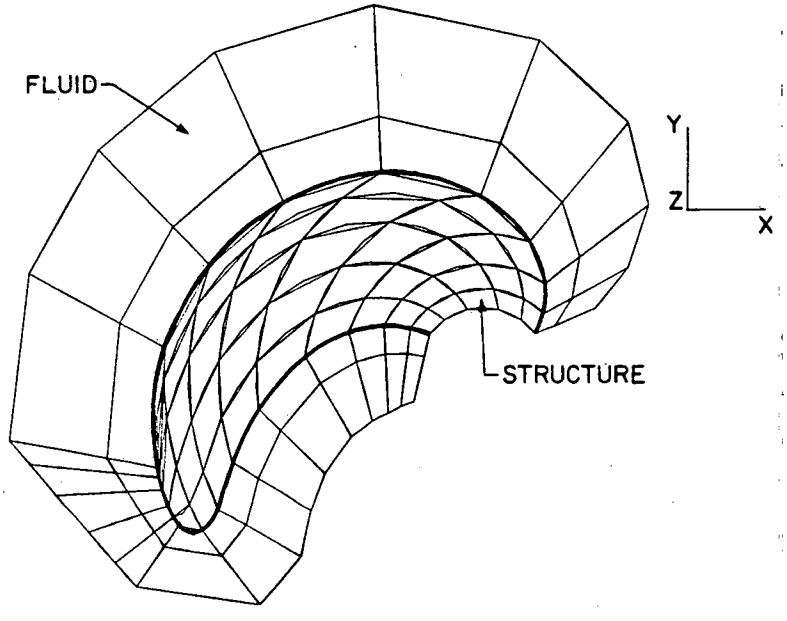

Figure 11: Finite element model of the P4388 propeller blade with a two layer fluid model.

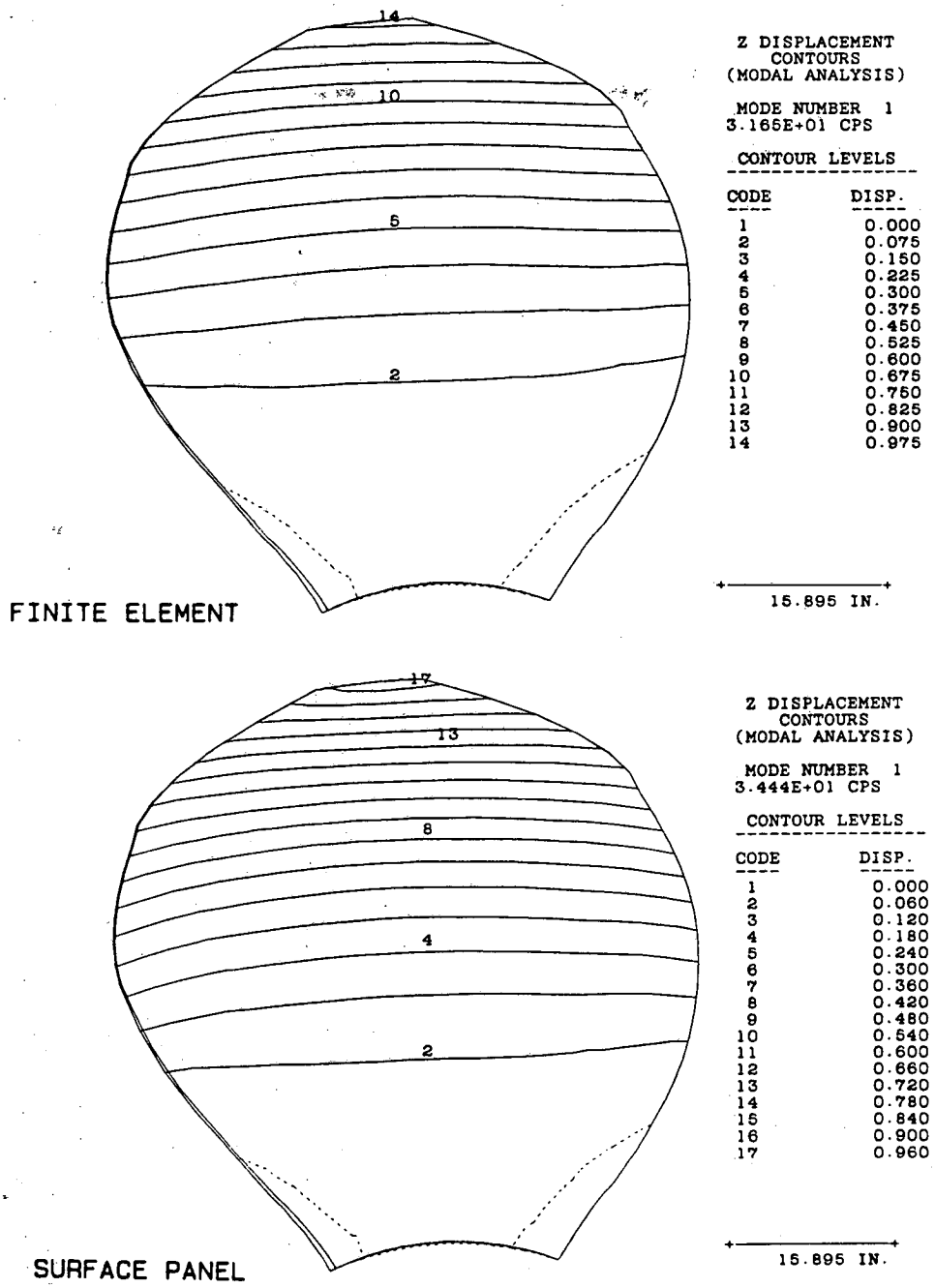

Figure 12: Mode 1 displacement contours for the DDH propeller blade for finite element and surface panel added mass matrices.

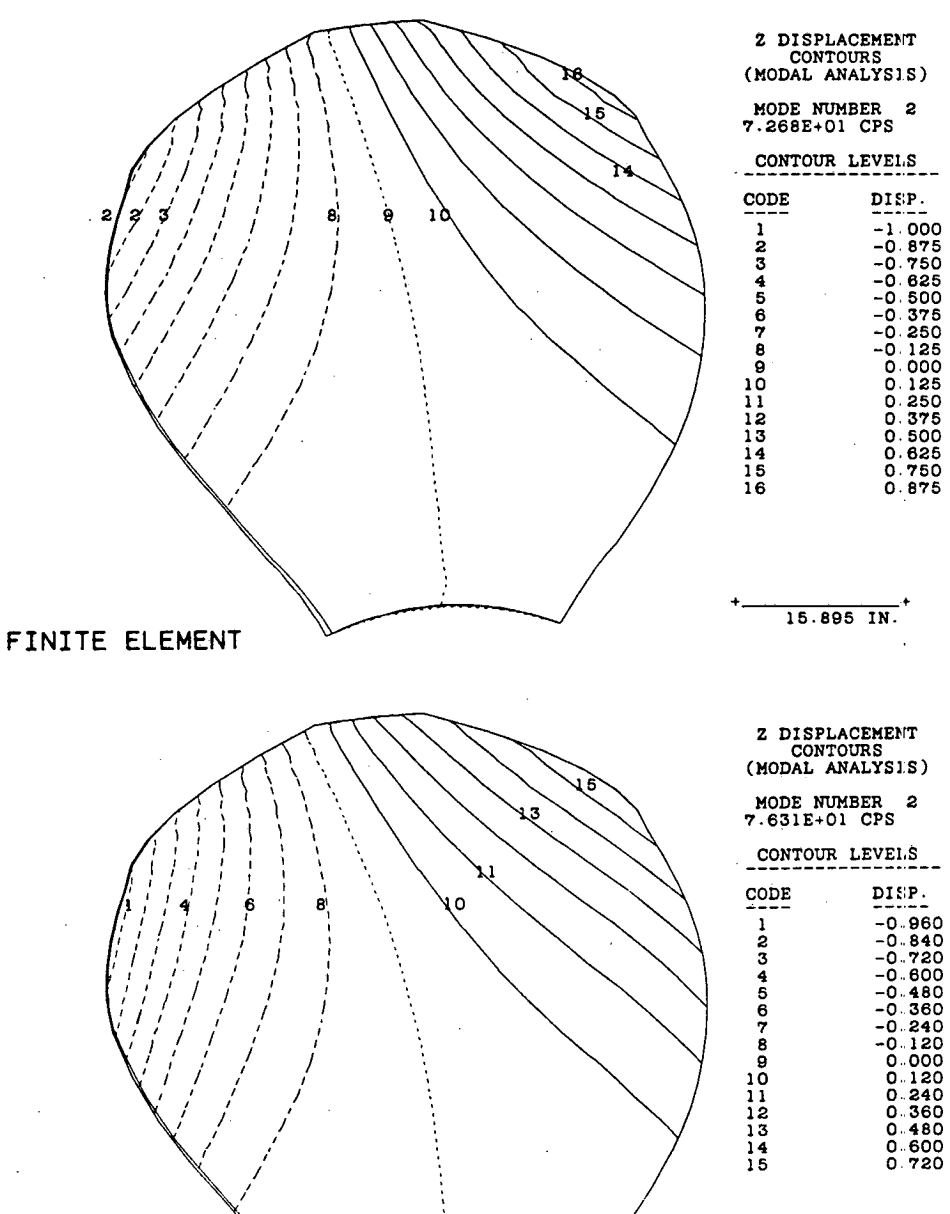

Figure 13: Mode 2 displacement contours for the DDH propeller blade for finite element and surface panel added mass matrices.

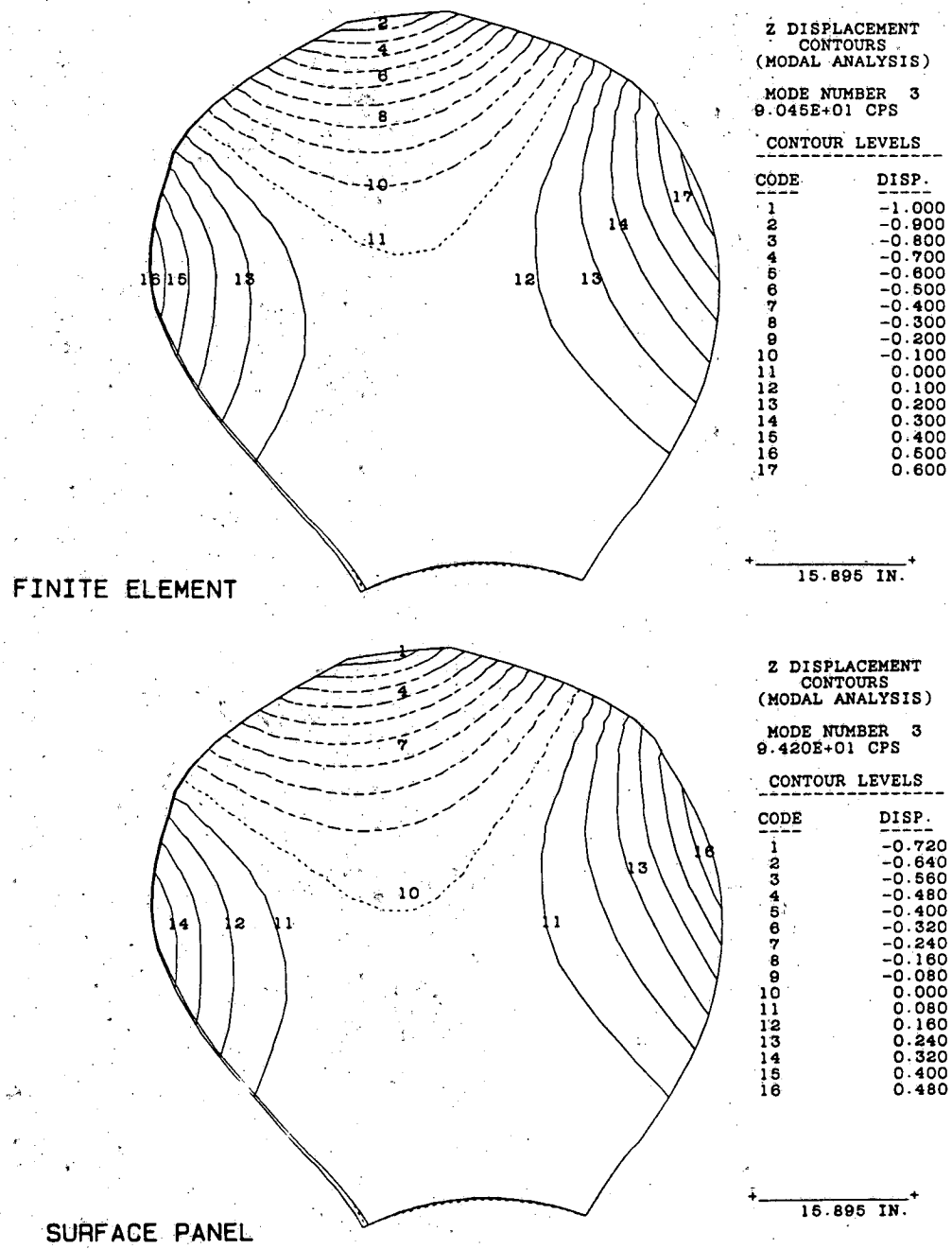

Figure 14: Mode 3 displacement contours for the DDH propeller blade for finite element and surface panel added mass matrices.

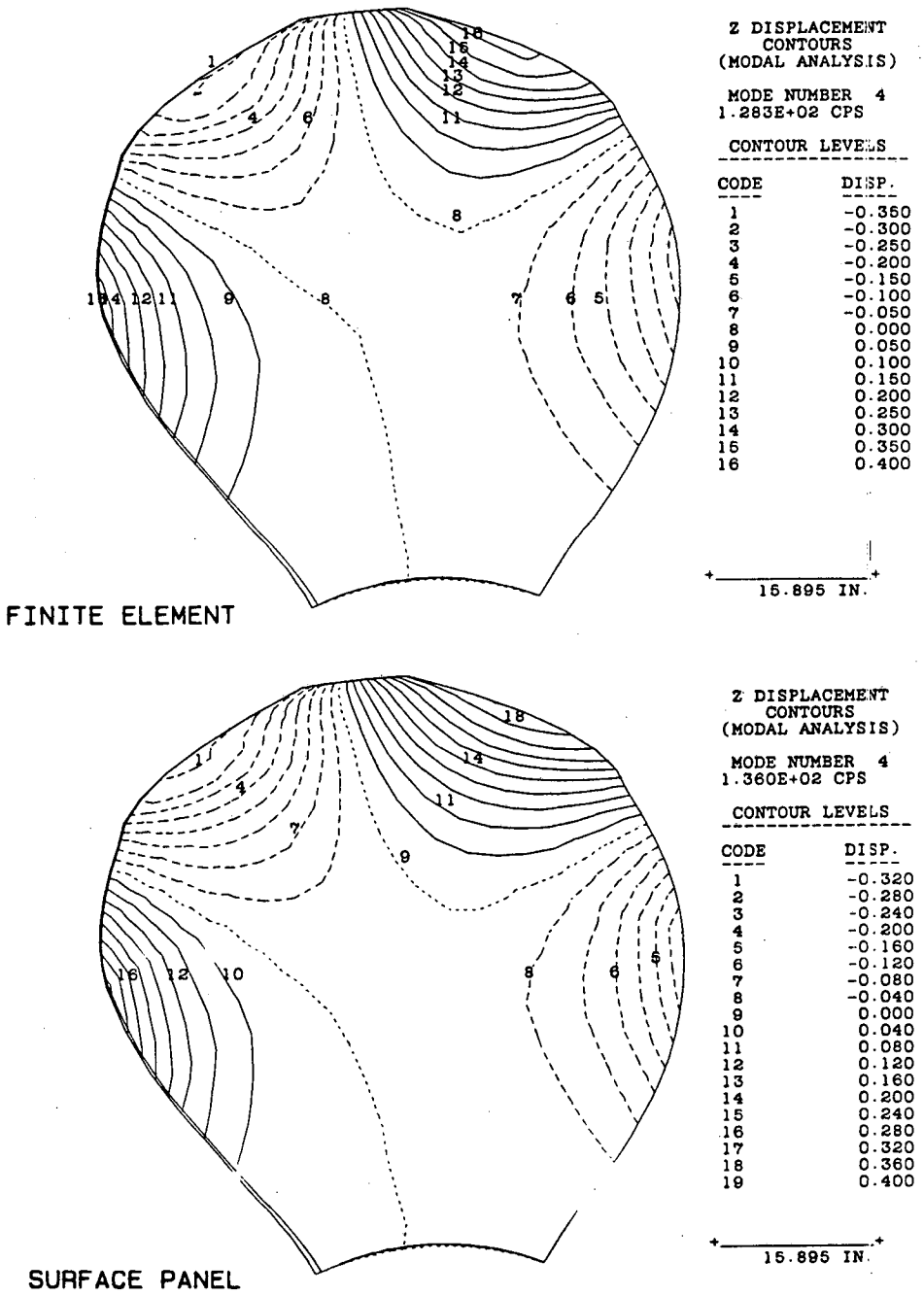

Figure 15: Mode 4 displacement contours for the DDH propeller blade for finite element and surface panel added mass matrices.

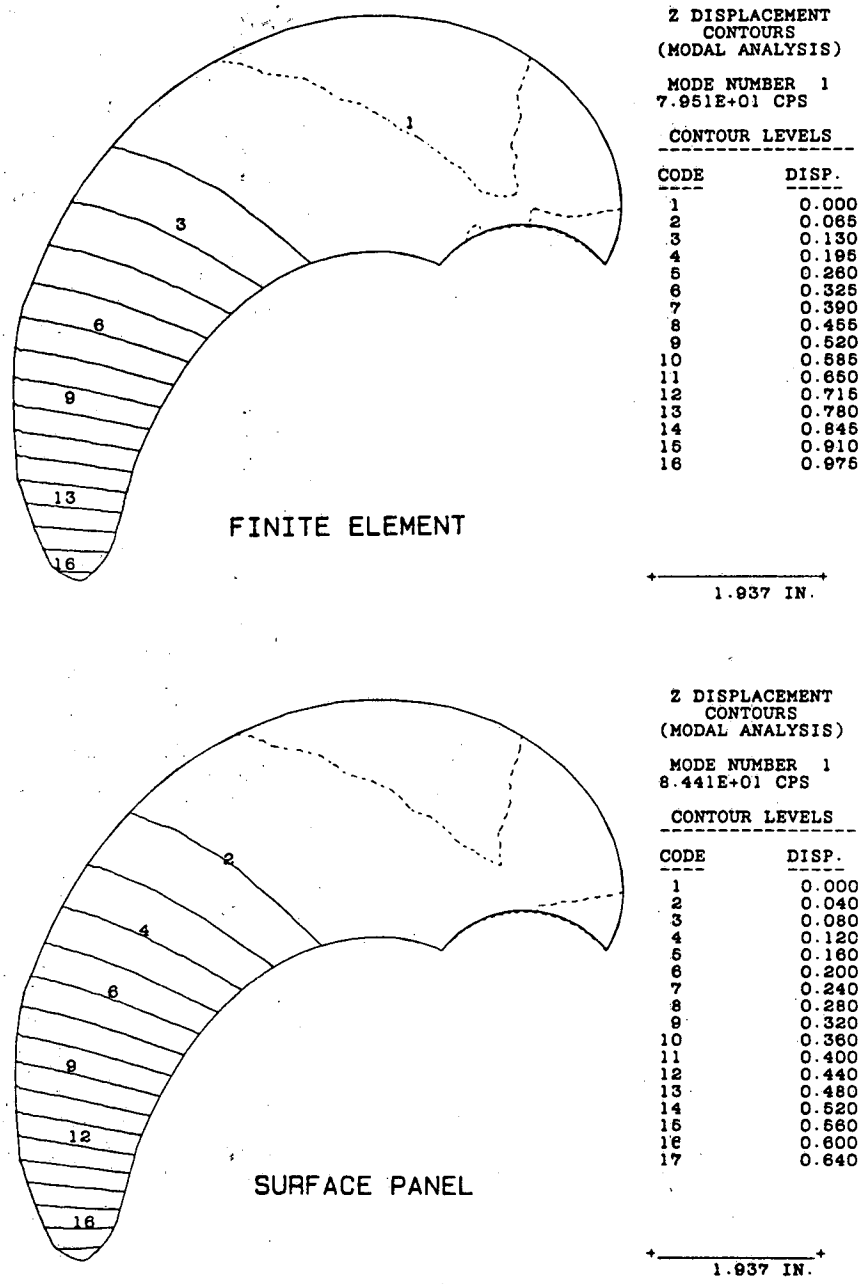

Figure 16: Mode 1 displacement contours for the P4388 propeller blade for finite element and surface panel added mass matrices.

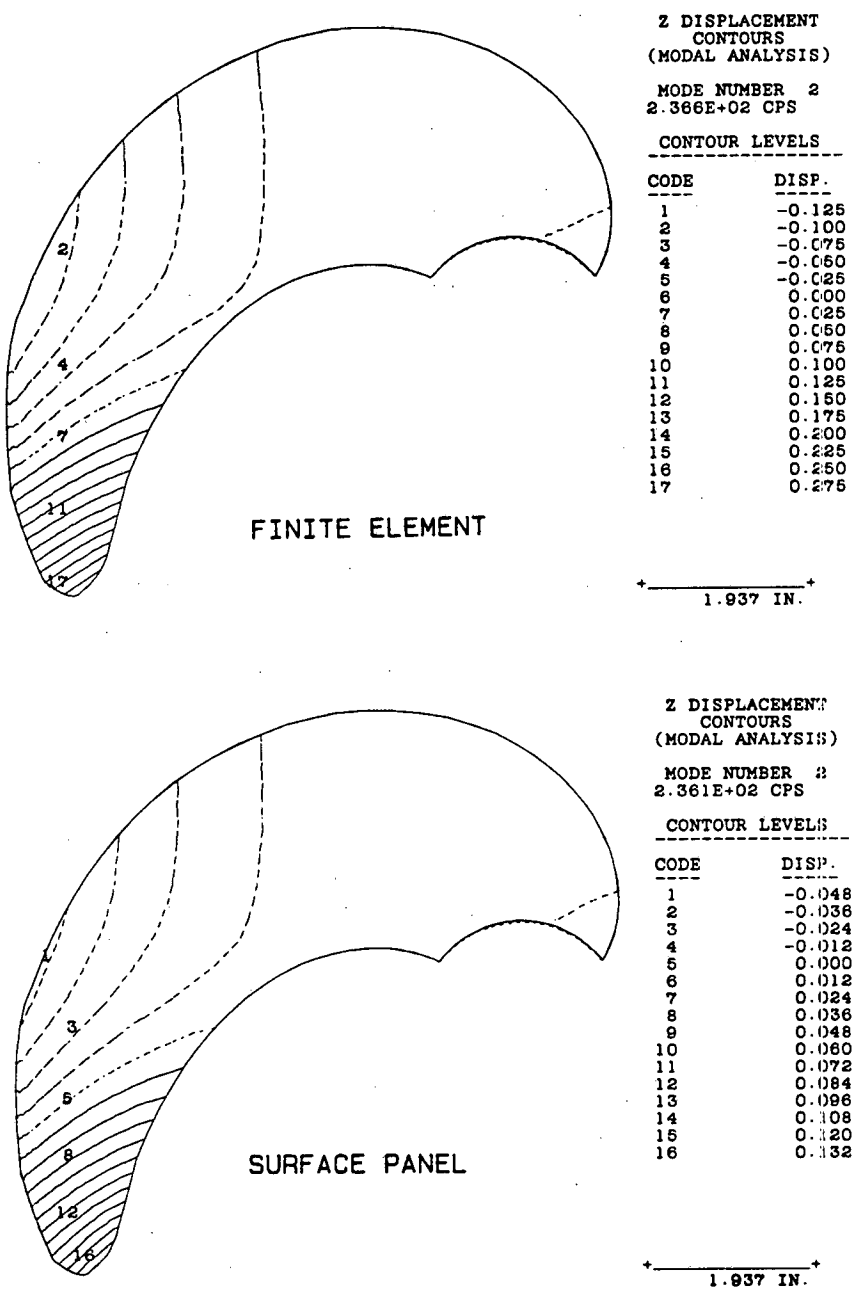

Figure 17: Mode 2 displacement contours for the P4388 propeller blade for finite element and surface panel added mass matrices.

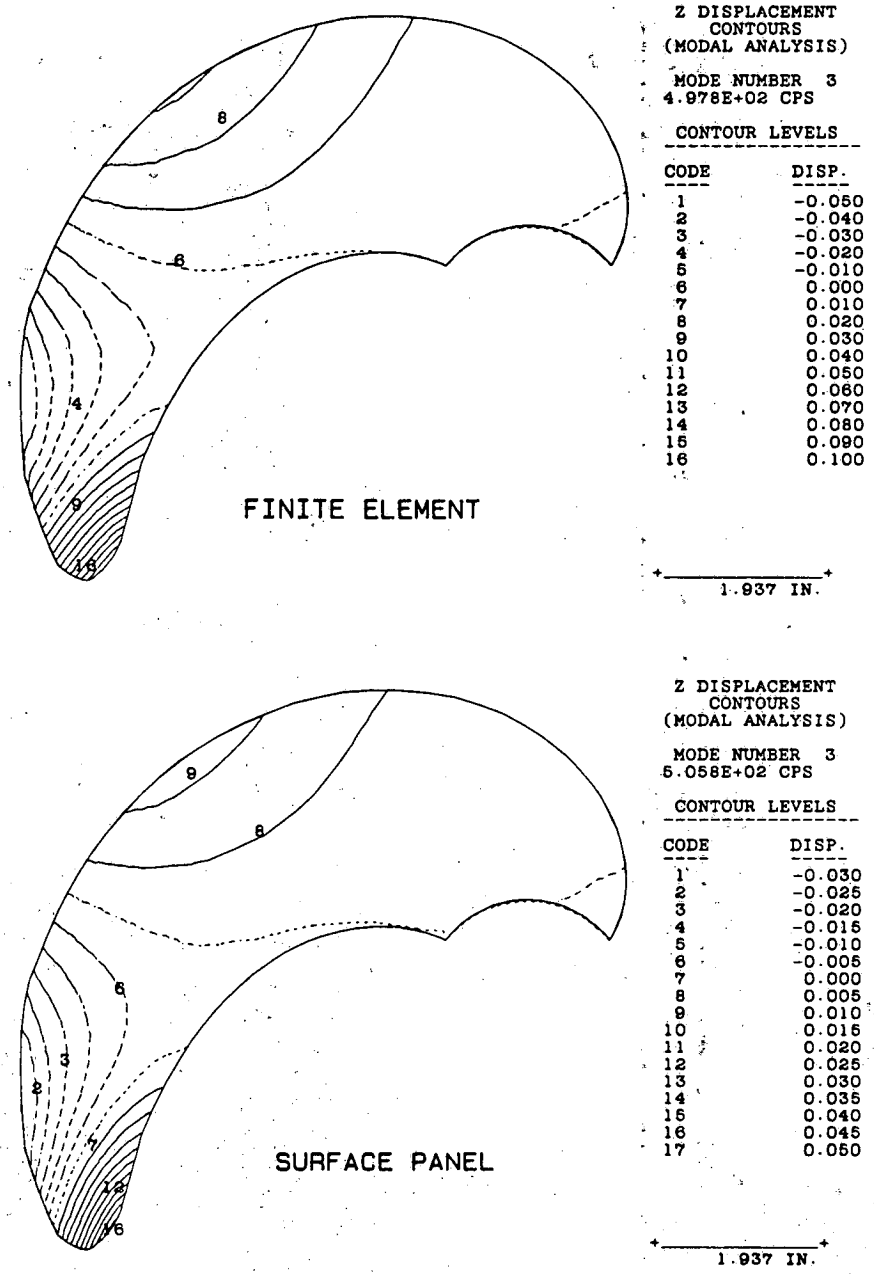

Figure 18: Mode 3 displacement contours for the P4388 propeller blade for finite element and surface panel added mass matrices.

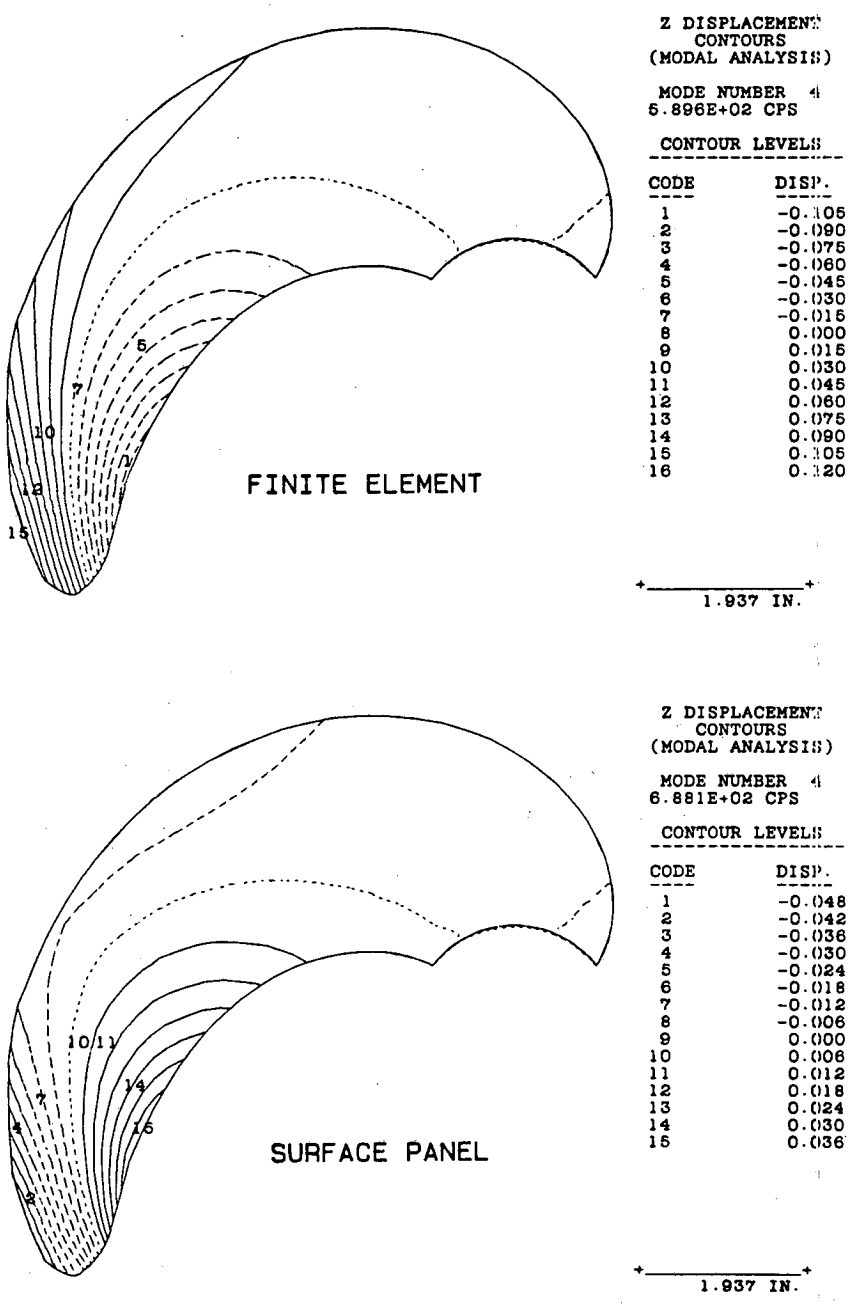

Figure 19: Mode 4 displacement contours for the P4388 propeller blade for finite element and surface panel added mass matrices.

Appendix A: Simplifying assumptions and boundary conditions

This appendix presents in more detail the assumptions inherent in the derivations of the linearized pressure and surface velocity terms, and the free surface boundary condition used in the surface panel formulation.

Pressure relation

The Navier-Stokes equations describe the fundamental equations of motion of a fluid. If we consider the velocity of a body through a stationary fluid to be equivalent to the motion of the fluid about a stationary body, the Navier-Stokes equation in the x direction for an ideal fluid is

$$\frac{\partial u^*}{\partial t} + u^*\frac{\partial u^*}{\partial x} + v^*\frac{\partial u^*}{\partial y} + w^*\frac{\partial u^*}{\partial z} = -\frac{1}{\rho}\frac{\partial p}{\partial x} \tag{31}$$

where $u^* = U + u$, etc., and U,V,W represent body velocities and u,v,w represent fluid disturbance velocities in the vicinity of the body. For an irrotational flow field, potential flow theory can then be used to define a velocity potential function Φ, where

$$\Phi = \phi_\infty + \phi \tag{32}$$

with

$$\phi_\infty = Ux + Vy + Wz \tag{33}$$

Here, ϕ is the disturbance potential in the fluid, and the disturbance velocities are defined as potential gradients

$$u = \frac{\partial \phi}{\partial x} \quad v = \frac{\partial \phi}{\partial y} \quad z = \frac{\partial \phi}{\partial z} \tag{34}$$

Substituting the velocity definitions into equation (31) and rearranging, we obtain

$$\frac{\partial^2 \phi}{\partial t \partial x} + (U+u)\frac{\partial^2 \phi}{\partial x^2} + (V+v)\frac{\partial^2 \phi}{\partial y \partial x} + (W+w)\frac{\partial^2 \phi}{\partial z \partial x} = -\frac{1}{\rho}\frac{\partial p}{\partial x} \tag{35}$$

Integrating equation (35) with respect to x, we obtain a pressure relation in the form

$$\frac{\partial \phi}{\partial t} + U\frac{\partial \phi}{\partial x} + V\frac{\partial \phi}{\partial y} + W\frac{\partial \phi}{\partial z} + \frac{1}{2}\left[(\frac{\partial \phi}{\partial x})^2 + (\frac{\partial \phi}{\partial y})^2 + (\frac{\partial \phi}{\partial z})^2\right] = -\frac{p}{\rho} \tag{36}$$

A linearized form of this relation for a body moving in the fluid can be obtained by neglecting the higher order terms. In addition, for a stationary body (equivalent to zero far field velocities U,V,W), this equation reduces to

$$p = -\rho\frac{\partial \phi}{\partial t} \tag{37}$$

which is the form used in the added mass matrix derivation given in this report.

Body surface boundary condition

The time derivatives involved in the body surface velocity boundary condition will also contain nonlinear terms when rigid body motion is included. The displacements of the body are defined by $\delta(x,y,z,t)$, for which the total derivative is

$$\frac{d\delta}{dt} = \frac{\partial\delta}{\partial t} + \frac{\partial\delta}{\partial x}\frac{dx}{dt} + \frac{\partial\delta}{\partial y}\frac{dy}{dt} + \frac{\partial\delta}{\partial z}\frac{dz}{dt} \tag{38}$$

Substituting the velocity components for the component time derivatives in (38), the full body surface velocity becomes

$$\frac{d\delta}{dt} = \frac{\partial\delta}{\partial t} + (U+u)\frac{\partial\delta}{\partial x} + (V+v)\frac{\partial\delta}{\partial y} + (W+w)\frac{\partial\delta}{\partial z} \tag{39}$$

The terms involving the disturbance velocities are commonly neglected on the basis of order of magnitude. Introducing the transformation matrix to relate global to normal directions, and recalling equation (3), the complete expression for the control point normal velocities is

$$\frac{\partial\phi}{\partial n} = [T]\{\dot{\delta}\} + U[T_1]\frac{\partial\delta}{\partial x} + V[T_2]\frac{\partial\delta}{\partial y} + W[T_3]\frac{\partial\delta}{\partial z} \tag{40}$$

Those terms involving rigid body velocities U,V,W in the pressure and surface boundary conditions (38) and (40) lead to additional terms in the nodal force vector. For example, the inclusion of a forward speed component U in the case of a ship hull has been considered in Reference 3. The complete expression for the force vector in that case becomes

$$\begin{aligned}\{F_f\} = &-\rho[T]^T[A][H][L]^{-1}[T]\{\ddot{\delta}\} \\ &- \rho U\left([T]^T[A][V_x][L]^{-1}[T] + [T]^T[A][H][L]^{-1}[T]\frac{\partial\{\delta\}}{\partial x}\right)\{\dot{\delta}\} \\ &+ \rho U^2\left([T]^T[A][V_x][L]^{-1}[T]\frac{\partial\{\delta\}}{\partial x}\right)\{\delta\}\end{aligned} \tag{41}$$

where $[V_x]$ is a coefficient matrix relating source strength to control point velocity in the x direction.

As can be seen from equation (41), the inclusion of the convective terms does not change the form of the added mass matrix. The second and third terms of the right-hand side can be considered added damping and added stiffness terms respectively. Their effect on the dynamic response of the structure is not considered in Reference 3, nor in the current report since the finite element system used in the analyses undertaken here does not include a capability to include a damping matrix in the above form. The added stiffness effects could be included; however, these terms are of higher order in δ, and are probably negligible at realistic forward speeds.

Free surface boundary condition

The definition of the free surface boundary condition represents perhaps the most serious approximation in both the finite element and surface panel formulation of the fluid/structure interaction problem. As discussed in Section 2, the surface panel method uses imaging of sources of opposite or similar sign across the plane of the free surface to define a zero potential (pressure relief) free surface, or a zero normal velocity free surface respectively. In the finite element method, the free surface nodes are normally specified as points of zero potential, providing again the pressure relief surface. These both represent approximations to the true free surface boundary condition, a discussion of which is presented below.

For a free surface which includes gravity waves, the equation of motion of the free surface is

$$\frac{dz}{dt} = -\frac{d\eta}{dt} \tag{42}$$

where $z = h + \eta$ and η is the wave amplitude, and h the depth of fluid. For potential flow, we have then the kinematic surface condition

$$\frac{d\eta}{dt} = -\frac{\partial \phi}{\partial z} \tag{43}$$

The pressure relationship from the Navier-Stokes equation, including the surface wave pressure, is

$$p = -\rho \frac{d\phi}{dt} + \rho g \eta \tag{44}$$

and at the free surface, where $p = 0$, equations (42), (43) and (44) can be combined to give

$$\frac{d^2\phi}{dt^2} + g\frac{\partial \phi}{\partial z} = 0 \tag{45}$$

Expanding the total derivative, and using again the potential flow relations (32) and (33) with

$$U = U_\infty \quad V = W = 0 \tag{46}$$

we obtain

$$\frac{\partial^2 \phi}{\partial t^2} + 2U_\infty \frac{\partial^2 \phi}{\partial x \partial t} + U_\infty^2 \frac{\partial^2 \phi}{\partial x^2} + g\frac{\partial \phi}{\partial z} = 0 \tag{47}$$

as the complete boundary condition. This condition is usually linearized in the sense that it is applied at $z = 0$, rather than at the dynamic free surface $z = \eta$. It is instructive to non-dimensionalize equation (47), using

$$\phi = \phi^* \phi_{scale} \quad t = \frac{t^*}{\omega} \quad x = x^* L \quad z = z^* L \tag{48}$$

Here, L is a characteristic length over which the potential varies, and ω a characteristic radial frequency. Substituting these relations into (47) and dropping the prime notation, we have

$$\frac{\omega^2 L}{g}\frac{\partial^2\phi}{\partial t^2} + \frac{2U_\infty\omega}{g}\frac{\partial^2\phi}{\partial x\partial t} + \frac{U_\infty^2}{gL}\frac{\partial^2\phi}{\partial x^2} + \frac{\partial\phi}{\partial z} = 0 \tag{49}$$

as the free surface boundary condition which the potential function ϕ must satisfy in addition to the Laplace equation and the body surface boundary condition. A simple solution does not exist for this problem, but under certain conditions, specific terms in equation (49) will be dominant, and a solution may be found which satisfies the simplified form of the boundary condition. Several cases are considered below.

Consider first a zero frequency limit, in which case (49) reduces to

$$\frac{U_\infty^2}{gL}\frac{\partial^2\phi}{\partial x^2} + \frac{\partial\phi}{\partial z} = 0 \tag{50}$$

A fundamental solution which satisfies this condition and the Laplace equation can be written in the form[19,20]

$$G = \frac{1}{r} - \frac{1}{r^*} + \frac{g}{\pi U_\infty^2}\int_{-\pi}^{\pi} d\theta \int_0^\infty f(x,y,z,k,\theta,)\, dk \tag{51}$$

in which k is the wave number and f is an exponential function. The extra term represents an integration of the wave-spectrum over the complete free surface. In the limit of zero forward speed, equation (51) can be shown to reduce to

$$G = \frac{1}{r} + \frac{1}{r^*} \tag{52}$$

which is exactly the condition obtained from the positive imaging system. This method thus satisfies exactly the boundary condition

$$\frac{\partial\phi}{\partial z} = 0 \tag{53}$$

in the zero frequency limit. As $U_\infty \to \infty$, equation (51) can be shown to reduce to

$$G = \frac{1}{r} - \frac{1}{r^*} \tag{54}$$

which is the condition obtained from the negative imaging system. The boundary condition

$$\frac{\partial^2\phi}{\partial x^2} = 0 \tag{55}$$

corresponding to a pressure relief surface is thus exactly satisfied in this case. Summarizing, for the $\omega = 0$ limit, the low Froude number problems can be approximated with the positive imaging method, and the higher Froude number problems with the negative imaging method.

In the case where $U_\infty = 0$ and $\omega \neq 0$, the free surface boundary condition becomes

$$\frac{\omega^2 L}{g}\frac{\partial^2 \phi}{\partial t^2} + \frac{\partial \phi}{\partial z} = 0 \tag{56}$$

Following the lines of the previous discussion, it can be seen that as $\omega \rightarrow 0$, the boundary condition can be satisfied exactly by the positive imaging method. As $\omega \rightarrow \infty$, the negative imaging system provides a correct representation.

The ADMASS system currently incorporates both the positive and negative imaging approach for the free surface approximation, and the above discussion indicates the types of problems for which the formulation will provide reasonable accuracy. In the general case in which neither limit is appropriate, the accuracy will depend on the relative magnitudes of the non-dimensional terms in the complete form of equation (49).

As an example, consider the magnitudes of the various terms which are relevant to an added mass calculation for a ship moving at a realistic forward speed. Take typical parameters as $U = 10\ m/sec, L = 5\ m$, (draft). As a function of ω, equation (49) becomes

$$0.51\omega^2\frac{\partial^2 \phi}{\partial t^2} + 2.04\omega\frac{\partial^2 \phi}{\partial x \partial t} + 2.04\frac{\partial^2 \phi}{\partial x^2} + \frac{\partial \phi}{\partial z} = 0 \tag{57}$$

For $\omega = 1.0 \ \ (f = 0.16Hz)$, all the terms are of the same order of magnitude, and poor accuracy could be expected from the imaging method. An order of magnitude dominance in the frequency dependent term relative to the final term is achieved for $\omega = 4.4 \ \ (f = 0.7Hz)$, and this would represent the approximate lower frequency limit for which the negative imaging system might be expected to provide adequate accuracy for these parameters. Since this limit is below the hull bending vibration frequencies of almost all ships, the negative imaging method will provide added fluid mass estimates valid for natural frequency or dynamic response analyses. The positive imaging approach appears to have little practical application to the computation of added fluid mass for vibrating structures as a free surface representation; the negative system has provided better agreement with other methods in all cases considered to date.

The incorporation of the more complex fundamental solution in the evaluation of the influence coefficients in the ADMASS system would involve a combination of both the current imaging system and an evaluation of the integral term of equation (51). This approach will necessitate the introduction of a numerical integration algorithm, and will add to the computational demand in that section of the system. The increased demand may be justified in cases where the limiting conditions satisfied by the imaging methods alone are not appropriate.

Appendix B - Surface Panel Integral Evaluation

In this appendix it is shown that the potential of a planar panel with uniform source distribution can be written in terms of expressions for the velocities induced by the same panel. The velocity relations were originally derived by Hess and Smith.[2]

The number of edges of the panel will be denoted N_e. Let $x_k, k = 1, \ldots, N_e$ denote the the corner points of the planar panel in clockwise order. A coordinate system is chosen so that the panel lies in the xy-plane; hence, $z_k = 0$.

The potential at $\mathbf{x} = (x, y, z)$ induced by a uniform unit source on the panel is

$$\phi(\mathbf{x}) = \int_{\Gamma_j} \frac{1}{|\mathbf{x} - \mathbf{x}'|}\, dx'dy' \tag{58}$$

where Γ_j denotes the panel surface. The associated velocity integral,

$$\mathbf{V}(\mathbf{x}) = \int_{\Gamma_j} \frac{\mathbf{x} - \mathbf{x}'}{|\mathbf{x} - \mathbf{x}'|^3} dx'dy' \tag{59}$$

has been solved exactly by Hess and Smith[2]

$$V_x = \sum_{k=1}^{N_e} V_{xk} \tag{60}$$

$$V_y = \sum_{k=1}^{N_e} V_{yk} \tag{61}$$

$$V_z = \sum_{k=1}^{N_e} \arctan\left(\frac{m_{k,k+1}e_k - h_k}{zr_k}\right) - \arctan\left(\frac{m_{k,k+1}e_{k+1} - h_{k+1}}{zr_{k+1}}\right) \tag{62}$$

where

$$V_{xk} = (y_{k+1} - y_k)\ln(R_k)/d_{k,k+1} \tag{63}$$

$$V_{yk} = -(x_{k+1} - x_k)\ln(R_k)/d_{k,k+1} \tag{64}$$

$$R_k = \frac{r_k + r_{k+1} - d_{k,k+1}}{r_k + r_{k+1} + d_{k,k+1}} \tag{65}$$

$$r_k = \sqrt{(x - x_k)^2 + (y - y_k)^2 + z^2} \tag{66}$$

$$e_k = (x - x_k)^2 + z^2 \tag{67}$$

$$h_k = (y - y_k)(x - x_k) \tag{68}$$

$$m_{k,k+1} = \frac{y_{k+1} - y_k}{x_{k+1} - x_k} \tag{69}$$

$$d_{k,k+1} = \sqrt{(x_{k+1} - x_k)^2 + (y_{k+1} - y_k)^2} \tag{70}$$

In these formulae it is understood that a subscript $N_e + 1$ on one of the corner points is equivalent to a subscript 1.

Consider the integral for the x-component of the velocity:

$$V_x(\mathbf{x}) = \int_{\Gamma_j} \frac{x - x'}{|\mathbf{x} - \mathbf{x}'|^3} dx'dy' \tag{71}$$

Let ∇ be the two dimensional gradient operator with respect to the primed coordinates.

$$\nabla \equiv \hat{x}\frac{\partial}{\partial x'} + \hat{y}\frac{\partial}{\partial y'} \tag{72}$$

Then

$$V_x(\mathbf{x}) = \int_{\Gamma_j} \nabla \cdot \left[\frac{\hat{x}}{|\mathbf{x} - \mathbf{x}'|}\right] dx'dy' \tag{73}$$

which, using the divergence theorem, can be reduced to a line integral counterclockwise around the perimeter of the panel.

$$V_x = \int_{\partial\Gamma_j} \frac{\hat{n} \cdot \hat{x}}{|\mathbf{x} - \mathbf{x}'|} ds \tag{74}$$

where $\partial\Gamma_j$ denotes the perimeter of the panel, ds is an increment of arclength, and $\hat{n}$ is an outward pointing unit normal to the perimeter.

The edge of the panel between $\mathbf{x}_k$ and $\mathbf{x}_{k+1}$ can be parameterized by

$$\mathbf{x}' = \mathbf{x}_k + (x_k - \mathbf{x}_{k+1})t \quad \text{for } t \in [-1, 0] \tag{75}$$

Note that the vertices must be passed in reverse order since the integral proceeds counterclockwise around the perimeter of the panel. The increment of arclength is then $ds = |x_{k+1} - \mathbf{x}_k|dt = d_{k,k+1}dt$. The normal is given by

$$\hat{n} = \frac{(\mathbf{x}_k - \mathbf{x}_{k+1}) \times \hat{z}}{d_{k,k+1}} \tag{76}$$

Therefore, $\hat{n} \cdot \hat{x} = (y_k - y_{k+1})dt$. Thus,

$$V_x = -\sum_{k=1}^{N_e} (y_{k+1} - y_k) \int_{-1}^{0} \frac{1}{|\mathbf{x} - \mathbf{x}'|} dt \tag{77}$$

Comparison with equations (60) and (63) shows that

$$\int_{-1}^{0} \frac{1}{|\mathbf{x} - \mathbf{x}'|} dt = -\frac{\ln(R_k)}{d_{k,k+1}} \tag{78}$$

Now consider the potential of equation (58). For reasons that will become clear shortly, rewrite the integral as follows.

$$\begin{aligned}\phi(\mathbf{x}) &= \int_{\Gamma_j} \frac{z^2+|\mathbf{x}-\mathbf{x}'|^2}{|\mathbf{x}-\mathbf{x}'|^3}dx'dy' - \int_{\Gamma_j} \frac{z^2}{|\mathbf{x}-\mathbf{x}'|^3}dx'dy' \\ &= \int_{\Gamma_j} \frac{z^2+|\mathbf{x}-\mathbf{x}'|^2}{|\mathbf{x}-\mathbf{x}'|^3}dx'dy' - zV_z \end{aligned} \tag{79}$$

Now

$$\begin{aligned}\frac{z^2+|\mathbf{x}-\mathbf{x}'|^2}{|\mathbf{x}-\mathbf{x}'|^3} &= \frac{2z^2+(x-x')^2+(y-y')^2}{|\mathbf{x}-\mathbf{x}'|^3} \\ &= -\nabla\cdot\left[\frac{(x-x')\hat{x}+(y-y')\hat{y}}{|\mathbf{x}-\mathbf{x}'|}\right] \end{aligned} \tag{80}$$

Using the divergence theorem again,

$$\begin{aligned}\phi(\mathbf{x}) &= -\int_{\partial\Gamma_j} \frac{\hat{n}\cdot[(x-x')\hat{x}+(y-y')\hat{y}]}{|\mathbf{x}-\mathbf{x}'|}ds - zV_z \\ &= -\int_{\partial\Gamma_j} \frac{\hat{n}\cdot(\mathbf{x}-\mathbf{x}')}{|\mathbf{x}-\mathbf{x}'|}ds - zV_z \end{aligned} \tag{81}$$

But, parameterizing the sides of the panel as before, one obtains

$$\begin{aligned}\hat{n}\cdot(\mathbf{x}-\mathbf{x}')ds &= [(\mathbf{x}_k-\mathbf{x}_{k+1})\times\hat{z}]\cdot(\mathbf{x}-\mathbf{x}')dt \\ &= [(\mathbf{x}-\mathbf{x}')\times(\mathbf{x}_k-\mathbf{x}_{k+1})]\cdot\hat{z}dt \\ &= [(\mathbf{x}-\mathbf{x}_k-(\mathbf{x}_k-\mathbf{x}_{k+1})t)\times(\mathbf{x}_k-\mathbf{x}_{k+1})]\cdot\hat{z}dt \\ &= [(\mathbf{x}-\mathbf{x}_k)\times(\mathbf{x}_k-\mathbf{x}_{k+1})]\cdot\hat{z}dt \\ &= [(x-x_k)(y_k-y_{k+1})-(y-y_k)(x_k-x_{k+1})]dt \end{aligned} \tag{82}$$

Therefore, making use of equations (78), (81), and (82),

$$\begin{aligned}\phi(\mathbf{x}) &= -zV_z + \sum_{k=1}^{N_e}[(x-x_k)(y_{k+1}-y_k)-(y-y_k)(x_{k+1}-x_k)]\int_{-1}^{0}\frac{1}{|\mathbf{x}-\mathbf{x}'|}dt \\ &= -zV_z - \sum_{k=1}^{N_e}[(x-x_k)(y_{k+1}-y_k)-(y-y_k)(x_{k+1}-x_k)]\frac{\ln(R_k)}{d_{k,k+1}} \\ &= -zV_z - \sum_{k=1}^{N_e}(x-x_k)V_{xk}+(y-y_k)V_{yk} \end{aligned} \tag{83}$$

Hence, the potential integral can be written in terms of the same algebraic expressions as the velocity integral. The extra computing time needed to calculate the potential integral in addition to the velocity integrals is very small.

Multipole Expansion for Large Separation

When the separation, r, of the panel and the field point considered is large, equations (58) and (59) can be expanded in terms of the small quantity $|\mathbf{x}'|/|\mathbf{x}|$. The general expression for the potential may be written as

$$\phi = \frac{I^{(0)}}{r} + \sum_{p\in(x,y)} I_p^{(1)} \frac{\partial}{\partial p}\left(\frac{1}{r}\right) + \sum_{p\in(x,y)} \sum_{q\in(x,y)} \frac{1}{2} I_{pq}^{(2)} \frac{\partial^2}{\partial p \partial q}\left(\frac{1}{r}\right) + \cdots \tag{84}$$

and for the velocity components as

$$\begin{aligned} V_p \;=\; -\Bigg[& I^{(0)} \frac{\partial}{\partial p}\left(\frac{1}{r}\right) + \sum_{q\in(x,y)} I_q^{(1)} \frac{\partial^2}{\partial p \partial q}\left(\frac{1}{r}\right) + \\ & \sum_{q\in(x,y)} \sum_{s\in(x,y)} \frac{1}{2} I_{qs}^{(2)} \frac{\partial^3}{\partial p \partial q \partial s}\left(\frac{1}{r}\right) + \cdots \Bigg] \quad \text{for } p \in (\mathbf{x},\mathbf{y},\mathbf{z}) \end{aligned} \tag{85}$$

where

$$I^{(0)} = \int_{\Gamma_j} dx'dy' \tag{86}$$

$$I_x^{(1)} = \int_{\Gamma_j} x'dx'dy' \quad ; \quad I_y^{(1)} = \int_{\Gamma_j} y'dx'dy' \tag{87}$$

$$I_{xx}^{(2)} = \int_{\Gamma_j} x'^2 dx'dy' \quad ; \quad I_{xy}^{(2)} = \int_{\Gamma_j} x'y'dx'dy' \quad ; \quad I_{yy}^{(2)} = \int_{\Gamma_j} y'^2 dx'dy' \tag{88}$$

and so on. The derivatives of $1/r$ are

$$\frac{\partial}{\partial p}\left(\frac{1}{r}\right) = -\frac{p}{r^3} \quad p \in (\mathbf{x},\mathbf{y},\mathbf{z}) \tag{89}$$

$$\frac{\partial^2}{\partial p \partial q}\left(\frac{1}{r}\right) = -\frac{\delta_{pq}}{r^3} + \frac{3pq}{r^5} \quad p,q \in (\mathbf{x},\mathbf{y},\mathbf{z}) \tag{90}$$

$$\frac{\partial^3}{\partial p \partial q \partial s}\left(\frac{1}{r}\right) = \frac{3p\delta_{qs}}{r^5} + \frac{3q\delta_{ps}}{r^5} + \frac{3s\delta_{pq}}{r^5} - \frac{15pqs}{r^7} \quad p,q,s \in (\mathbf{x},\mathbf{y},\mathbf{z}) \tag{91}$$

where δ_{pq} is the Kronecker delta. Note that the panel moments $\mathbf{I}^{(n)}$ are properties of the panel alone: they do not depend upon the point at which the velocity is to be evaluated. Details of the method by which they are evaluated in the ADMASS system are given by Hally.[21] The origin of the panel coordinates has been chosen to be the centroid of the panel so that $I_x^{(1)} = I_y^{(1)} = 0$; hence, the second term in the expansion vanishes. This choice also

ensures that the multipole expansion can be used whenever r is much larger than the mean dimensions of the panel. Up to third order,

$$\phi \approx \frac{I^{(0)}}{r} + \frac{(3x^2 - r^2)I_{xx}^{(2)}}{2r^5} + \frac{3xyI_{xy}^{(2)}}{r^5} + \frac{(3y^2 - r^2)I_{yy}^{(2)}}{2r^5} \tag{92}$$

and

$$V_x \approx \frac{xI^{(0)}}{r^3} - \frac{3x(3r^2 - 5x^2)I_{xx}^{(2)}}{2r^7} - \frac{3y(r^2 - 5x^2)I_{xy}^{(2)}}{r^7} - \frac{3x(r^2 - 5y^2)I_{yy}^{(2)}}{2r^7} \tag{93}$$

$$V_y \approx \frac{yI^{(0)}}{r^3} - \frac{3y(r^2 - 5x^2)I_{xx}^{(2)}}{2r^7} - \frac{3x(r^2 - 5y^2)I_{xy}^{(2)}}{r^7} - \frac{3y(3r^2 - 5y^2)I_{yy}^{(2)}}{2r^7} \tag{94}$$

$$V_z \approx \frac{zI^{(0)}}{r^3} - \frac{3z(r^2 - 5x^2)I_{xx}^{(2)}}{2r^7} - \frac{15xyzI_{xy}^{(2)}}{r^7} - \frac{3z(r^2 - 5y^2)I_{yy}^{(2)}}{2r^7} \tag{95}$$

In the ADMASS system, the exact solutions corresponding to equations (60), (61), (62) and (83) are used when r is small. At moderate separations, the first three term expansions of the expansions of equations (93)-(95) are utilized. At large separations, the first term of those expansions is utilized in the integral evaluation.

Appendix C - Program Execution

This appendix describes the input requirements and program prompts in the ADMASS system. The system can be run interactively as a series of programs ADMS1 - ADMS4, or as a single system from a command file in batch mode. The interactive form will be discussed here: the necessary responses are the same in either approach.

The ADMASS system begins with the ADMS1 routine, which accesses the structural and fluid geometry files PREFIX.GOM and PREFIX.AMD. The format of these files should be exactly as described in Reference 5, with the exception that the first element group in the .AMD file must contain all of the interface elements. Mixing of interface element types is not permitted at the present time, and only element types 1 and 3 are permitted. The .GOM file need only contain the structural nodal coordinates since element definitions are not read. The ADMS1 routine rarely takes more than a few seconds of CPU time for completion. The prompts and expected responses (in brackets - use capitals) for this routine are as follows.

Enter 5 character prefix of VAST files (Character)

Reverse the interface node order? (Y,N)

If the response to the second prompt is Y, the corner node numbering of all panels will be reversed from that defined in the .AMD file. This causes a reversal in the panel normal orientation in the event that connectivity has been input consistently in reverse order. To avoid the necessity of this option, panels should be defined in a counter-clockwise sense viewed from the fluid.

Are interface elements uniquely defined? (Y,N)

This option is necessary when the thin body assumption has been used in the interface element definitions and a second surface needs to be generated. If all panels would correspond to a unique fluid element, this option is not required. If the panels are not unique, several options will be presented:

Are solid elements used in structure? (Y,N)

If 20-node solid elements have been used to model the structure, the second surface can be defined by specifying node number increments for the corner and midside nodes of the available surface. These increments will require some knowledge of the model generation system, and the validity of the second surface is obviously dependent on the compatibility

of the node numbering system with this algorithm. The prompts for this option are

Enter corner node increment for surface 2 (Integer)
Enter midside node increment for surface 2 (Integer)

One other option is available for generation of the second surface in the case that shell element modelling option 1 has been used in the structural model (see Reference 1 pp. C2-E1.4). This option appears if N has been entered in response to the solid element prompt above.

Shell element option 1 used? (Y,N)

If Y is entered here, the program automatically uses the parameter NDN (number of displacement nodes) defined in the .GOM file as the nodal increment for all surface 1 nodes. This again is not a generally applicable approach, but has been developed with the solid modelling option to be compatible with current versions of the propeller modelling system.[15] If neither solid nor shell element option 1 has been used in the model, a second surface must be defined by alternative means.

In all cases where the 8-node interface element has been used, two refinement options are available:

Edge 1 panel refinement required? (Y,N)
Edge 2 panel refinement required? (Y,N)

These options divide each panel defined in the .AMD file into two elements, using the midside nodes of two opposite edges and the 4 corner nodes. Only one of these options can be used at a time, since an additional node within the interface element would be required for refinement in both directions. Edge 1 of an element is defined by the first 2 nodes in the interface element definition; edge 2 is defined by the second and third nodes (see Figure 5).

The program should now return the following information:

Fluid geometry file read completed.
Number of panels is:__
Number of interface nodes is:__

These values should be checked against expectations to determine if the refinement algorithms are working properly.

A header for identifying output disc files will now be required,

Enter a title for identifying output files (Character)

Since all file names are fixed within the ADMASS system and the files are in binary form, the header serves as the only check in subsequent routines that the correct files are being used.

Panel properties are now calculated, and the following lines should appear as calculations proceed

Calculating panel properties...
Panel Property and Transform files written.
Exiting ADMS1..

The output files are titled PANPRP.MAS and TMTRX.MAS respectively. Several error checks are made during the panel property calculations. The most common error is the nodal connectivity definition, which can usually be corrected with the node reversal option. If errors in element connectivity result in non-quadrilateral shapes, the error message

The control point of panel ( ) does not lie within the panel boundaries

will usually be triggered. To facilitate debugging of interface grids, the ADMS1 routine writes the interface element nodes (by element), the panels a particular node is connected to (by node) and the panel corner coordinates, area, and normal components to a formatted disc file ADMS1.DAT.

The ADMS2 program can be run on successful completion of the ADMS1 routine. This program calculates the influence coefficients relating the panel source strength to control point (panel centroid) velocity potential and normal velocity. This system is quite efficient, but can take several minutes of CPU time for a larger problem ($\geq$ 200 panels). The following information and prompts should appear:

Entering ADMS2...

Reading panel properties from PANPRP.MAS ... Done

Header is:
Prefix _____ Time, Date

Enter free surface boundary condition

1. **1/R + 1/R' : Symmetry reflection of structure across surface.**
2. **1/R - 1/R' : Pressure release boundary.**
3. **No free surface.**

The response to this prompt is dependent on the particular problem. In all cases considered to date, option 2 has provided a better approximation to the free surface than option 1. If the body is completely submerged, option 3 is required. The next prompt,

Calculate influence coefficients for velocity components? (Y,N)

defines influence coefficient matrices unrelated to the added mass problem, and a N response should be entered here. The symmetry option may be used,

X-Z plane of symmetry? (Y,N)

for half models, noting again the specific coordinate system that is used within the program. A further prompt concerning antisymmetric influence coefficient matrices

Calculate antisymmetric influence coefficients? (Y,N)

can also be answered N for an added mass calculation. The ADMS2 program then begins the calculation of the influence coefficient matrices, informing the user of progress on an ongoing basis. The binary output files of this routine are INFPHI.MAS and INFCFF.MAS.

The ADMS3 program inverts the matrix stored on the disc file INFCFF.MAS, producing the file INVERS.MAS. This is generally the lengthiest section of the added mass matrix generation. The minimum CPU time demand of the current algorithm is proportional to between $(NP)^2$ and $(NP)^3$, where NP is the number of surface panels. The actual CPU time will depend on the convergence performance for the matrix being inverted. For models with fluid on one side only, the CPU time is usually quite close to the minimum.

The method uses Gauss elimination and back substitution in the solution of blocks along the matrix diagonal; the number of blocks is the only input to this routine. In test runs, an optimum efficiency appears to be obtained when the block size is 10 to 15 percent of the matrix dimension. The solutions of these blocks are then used in a Seidel form of iterative solution, using the identity vectors as right-hand sides.

The ADMS3 routine will print an iteration count when the number of iterations for convergence of any vector exceeds five. If poor convergence performance is indicated by the routine, a restart with a smaller number of blocks is recommended. The maximum number of iterations performed within the routine is twenty; if this count is indicated in the statistics, the run should be aborted.

The following format should appear when this program is run:

Entering ADMS3....

Total number of panels = ___

Enter number of blocks desired for decomposition
(Maximum is 40 - 0 for default) (Integer)

The number of blocks need not be a round divisor of the matrix size NP. On entry of the desired number of blocks, the program informs the user of progress on an ongoing basis. If the iteration count for any vector exceeds five, the following message will be printed:

Poor convergence performance for this matrix: ___ iterations required

The tolerance sought in the iteration is less than 0.001 in the current version. This error limit has little effect on the accuracy of the added mass matrix for well conditioned coefficient matrices, but can drastically increase the CPU time required for matrix inversion. The current setting is considered to be a good balance between accuracy and computational efficiency, and thus has not been made an interactive variable.

The final routine in the ADMASS calculation suite is the ADMS4 program, which performs a series of matrix multiplications to produce the fluid added mass matrix. As discussed in Section 2 of this report, the source and dipole formulations of the surface panel method represent different multiplication orders, and the option for one or the other is given here. This routine can be reasonably CPU intensive, often taking about 2/3 the CPU time used by the ADMS3 program. The inputs to this routine are the panel formulation desired and the density of the fluid. The program uses the files TMTRX.MAS, INFPHI.MAS, and INVERS.MAS; again, progress statements are given as operations are begun and completed. The output of this routine is the fluid mass matrix PREFIX.T36, compatible with the VAST finite element analysis system.

Post-processing options to read selected entries in the added mass matrix, compute rigid body masses, condense or to symmetrize the matrix have been incorporated in a program ADMSP. For matrix condensation, the program accesses the TMTRX.MAS file for information on the number of displacement nodes. A warning is given to ensure that the TMTRX.MAS matrix corresponds to the added mass matrix being reduced. The prompts for this program are

Enter name of T36 file to read (5 character prefix)

Enter post-processing option required

1: Read selected entries in the matrix
2: Rigid body mass additions
3: Reduction to displacement nodes
4: Symmetrize mass matrix
5: Stop

In cases where both a reduction and symmetrization are desired, the reduction should be done first, and this menu will be offered on completion of the reduction. The program will allow only one reduction of the mass matrix. The reduction process is quite CPU intensive, and will take up to about 20 percent of the CPU time required to create the mass matrix. The symmetry option is not CPU demanding.

References

1. 'Studies on Fluid Structural Vibration Using Boundary Element Method', Mitsubishi Technical Bulletin No. 172, June, 1986.

2. Hess A.M.O., Smith J.L., 'Calcualtion of Non-lifting Potential Flow About Arbitrary Three-dimensional Bodies', Report E.S. 40622, Douglas Aircraft Co., 1962.

3. Vorus W.S., Hylarides S., 'Hydrodynamic Added-Mass Matrix of Vibrating Ship Based on a Distribution of Hull Surface Sources', Trans. SNAME, Vol. 89, 1981, pp. 397-416.

4. Hylarides S., Vorus, W.S., 'The Added Mass Matrix in Ship Vibration Using a Source Distribution Related to the Finite Element Grid of the Ship Structure', Int. Shipbuilding Progress, Vol. 29, No. 330, 1982.

5. 'Vibration and Strength Analysis Program VAST, Version 4, User Manual', DREA Contract Report CR86/429, Martec Ltd. 1986.

6. Lee J., 'A Potential Based Panel Method for the Analysis of Marine Propeller Blades in Steady Flow', Report 87-13, Massachusetts Institute of Technology, Department of Ocean Engineering, Cambridge, Mass., 1987.

7. Norwood M., 'Application of the Finite Element Method for the Calculation of the Hydrodynamic Added Mass of Marine Propeller Blades', DREA Informal Communication, 1977.

8. Hally D., 'POTFLO - A Suite of Programs for Calculating Potential Flow About Ship Hulls', DREA Technical Memorandum, in review.

9. Sarpkaya, T., Isaacson, M., Mechanics of Wave Forces on Offshore Structures, Van Nostrand Reinhold, New York, 1981.

10. Lewis, F. M., 'The Inertia of Water Surrounding a Vibrating Ship', Trans. SNAME, Vol. 37, 1929, pp. 1-20.

11. Hicks, A. N., 'The Theory of Explosion Induced Ship Whipping Motions', Naval Construction Research Establishment Report R579, Dunfermline, U.K., 1972.

12. Hally D., 'Numerical Approximation of Ship Hulls', DREA Technical Memorandum TM85/207, 1985.

13. Hally D., 'Representation of Hulls with Knuckles', DREA Technical Memorandum TM86/209, 1986.

14. Glenwright D., Hutton S., 'Experimental and Finite Element Investigation of Added Mass Effects on Ship Structures', DREA Contract Report CR87/464, 1987.

15. 'Vibration and Stress Analysis of Marine Propellers by Finite Element Methods', DREA Contract Report, Martec Ltd., 1983.

16. Smith D.R., Slater J.E., DREA RN/H/79/4, Informal Communication.

17. Slater J.E., Smith D.R., 'Prediction of Static Stress, Natural Frequencies and Mode Shapes for the DTNSRDC 4388 Highly Skewed Propeller Blade by Finite Element Analysis', DREA RN/H/82/19, Informal Communication.

18. Dhir S.K., Sikora J.P.,' Holographic Study of Vibration Characteristics of a Highly Skewed Propeller Blade Model', DTNSRDC Technical Note 193, August, 1971.

19. Doctors J.L., Beck R.F., 'Numerical Aspects of the Neumann-Kelvin Problem', J. of Ship Research, Vol. 31, No. 1, March 1987, pp. 1-13.

20. Wehausen J.V., Laitone, E.V., 'Surface Waves,' Encyclopedia of Physics, Vol. 9, Flugge, Ed. Springer Verlag, Berlin,1960.

21. Hally D., 'Calculation of the Moments of Polygons', DREA Technical Memorandum TM87/209, 1987.

Unclassified

SECURITY CLASSIFICATION OF FORM
(highest classification of Title, Abstract, Keywords)

DOCUMENT CONTROL DATA

(Security classification of title, body of abstract and indexing annotation must be entered when the overall document is classified)

1. ORIGINATOR (the name and address of the organization preparing the document. Organizations for whom the document was prepared, e.g. Establishment sponsoring a contractor's report, or tasking agency, are entered in section 8.)

Defence Research Establishment Atlantic

2. SECURITY CLASSIFICATION (overall security classification of the document, including special warning terms if applicable)

Unclassified

3. TITLE (the complete document title as indicated on the title page. Its classification should be indicated by the appropriate abbreviation (S,C,R or U) in parentheses after the title.)

A SURFACE PANEL METHOD FOR THE CALCULATION OF ADDED MASS MATRICES FOR FINITE ELEMENT MODELS

4. AUTHORS (Last name, first name, middle initial. If military, show rank, e.g. Doe, Maj. John E.)

Vernon, T.A., Bara, B., Hally, D.

5. DATE OF PUBLICATION (month and year of publication of document)

February 1988

6a. NO. OF PAGES (total containing information. Include Annexes, Appendices, etc.)

65

6b. NO. OF REFS (total cited in document)

21

6. DESCRIPTIVE NOTES (the category of the document, e.g. technical report, technical note or memorandum. If appropriate, enter the type of report, e.g. interim, progress, summary, annual or final. Give the inclusive dates when a specific reporting period is covered.)

DREA Technical Memorandum

8. SPONSORING ACTIVITY (the name of the department project office or laboratory sponsoring the research and development. Include the address.)

9a. PROJECT OR GRANT NO. (if appropriate, the applicable research and development project or grant number under which the document was written. Please specify whether project or grant)

9b. CONTRACT NO. (if appropriate, the applicable number under which the document was written)

10a. ORIGINATOR'S DOCUMENT NUMBER (the official document number by which the document is identified by the originating activity. This number must be unique to this document.)

DREA TECH. MEMORANDUM 88/203

10b. OTHER DOCUMENT NOS. (Any other numbers which may be assigned this document either by the originator or by the sponsor)

11. DOCUMENT AVAILABILITY (any limitations on further dissemination of the document, other than those imposed by security classification)

- (X) Unlimited distribution
- ( ) Distribution limited to defence departments and defence contractors; further distribution only as approved
- ( ) Distribution limited to defence departments and Canadian defence contractors; further distribution only as approved
- ( ) Distribution limited to government departments and agencies; further distribution only as approved
- ( ) Distribution limited to defence departments; further distribution only as approved
- ( ) Other (please specify):

12. DOCUMENT ANNOUNCEMENT (any limitation to the bibliographic announcement of this document. This will normally correspond to the Document Availabilty (11). However, where further distribution (beyond the audience specified in 11) is possible, a wider announcement audience may be selected.)

Unlimited

Unclassified

SECURITY CLASSIFICATION OF FORM

DCD03 2/06/87

13. ABSTRACT (a brief and factual summary of the document. It may also appear elsewhere in the body of the document itself. It is highly desirable that the abstract of classified documents be unclassified. Each paragraph of the abstract shall begin with an indication of the security classification of the information in the paragraph (unless the document itself is unclassified) represented as (S), (C), (R), or (U). It is not necessary to include here abstracts in both offical languages unless the text is bilingual).

A method of generating the added fluid mass matrix for use in dynamic analyses of submerged structures is presented. This method uses a distribution of panel singularities in the form of sources or dipoles on the fluid/structure interface to represent the velocity potential in the fluid surrounding the structure. The fluid added mass matrix is calculated by relating the pressure field in the fluid to the structure surface accelerations via the Euler equation and the assumptions of potential flow theory. Based on the results of a variety of investigations of computational performance, convergence and dynamic response involving floating cylinders, ship hulls, and propeller blades, the surface panel method is shown to provide an effective alternative to the finite element added mass matrix system. The surface panel program suite has been developed in a form compatible with an existing finite element analysis package, although the dependence on the particular solution system is not large.

14. KEYWORDS, DESCRIPTORS or IDENTIFIERS (technically meaningful terms or short phrases that characterize a document and could be helpful in cataloguing the document. They should be selected so that no security classification is required. Identifiers, such as equipment model designation, trade name, military project code name, geographic location may also be included. If possible keywords should be selected from a published thesaurus. e.g. Thesaurus of Engineering and Scientific Terms (TEST) and that thesaurus-identified. If it is not possible to select indexing terms which are Unclassified, the classification of each should be indicated as with the title.)

Mass matrix
Added mass
Fluid/structure interaction
Interaction
Dynamics
Finite element
Panel
Surface panel
Boundary integral
Potential flow

#55028